

Variational free oscillation computations for three laterally heterogeneous Earth models

Sandra P. Morris^{1*}, Robert J. Geller^{1,2}, Hitoshi Kawakatsu^{1**}
and Seiji Tsuboi²

¹ *Department of Geophysics, Stanford University, Stanford, California 94305 (U.S.A.)*

² *Department of Geophysics, Faculty of Science, Tokyo University, Bunkyo, Tokyo, 113 (Japan)*

(Received April 9, 1986; revision accepted October 1, 1986)

Morris, S.P., Geller, R.J., Kawakatsu, H. and Tsuboi, S., 1987. Variational free oscillation computations for three laterally heterogeneous Earth models. *Phys. Earth Planet. Inter.*, 47: 288–318.

The eigenfrequencies and eigenfunctions of the modes of three laterally heterogeneous, anelastic, elliptical, rotating models are calculated using the variational method. The basis set consists of the degenerate singlets of 11 multiplets of a spherically symmetric model (four toroidal and seven spheroidal multiplets), giving a total of 351 trial functions. The eigenfrequencies of the degenerate multiplets are clustered in a narrow frequency band around 250 s. The solution of the resulting 351×351 complex, non-hermitian eigenvalue problem required about 30 s of CPU time on the Hitachi S-810/20 supercomputer at the Computer Centre of Tokyo University. The power of present computational facilities thus makes the variational method a practical approach for studying the Earth's lateral heterogeneity. Using results presented elsewhere, the variational method can be used to obtain the partial derivatives of the eigenfrequencies with respect to a change in an initially laterally heterogeneous model.

The eigenfrequencies and eigenfunctions of the more accurate variational calculation substantially differ from those of first order degenerate perturbation theory, which does not include coupling between multiplets. Our basis set includes ${}_0S_{32}$ and ${}_0T_{31}$, which are well-known to be coupled by Coriolis terms. However, the results of the variational calculations show that the degree of coupling between these two fundamental mode multiplets is comparable to their coupling with nearby overtone multiplets that results from lateral heterogeneity.

Synthetic line spectra (without anelastic attenuation) are calculated for two earthquakes: the 1977 Indonesia event and a 1978 deep event of Honshu, Japan, for the three laterally heterogeneous Earth structure models. There are marked differences between the line spectra for three Earth models, and between the line spectra for the variational method and those from first order degenerate perturbation theory for a given Earth model. In contrast, when anelastic attenuation is included in the calculation of the synthetic spectra, the differences between Earth models, and between perturbation theory and the variational method, become much less distinct. Resolving the Earth's lateral heterogeneity is thus likely to require the processing of large amounts of data in order to overcome the effects of anelasticity.

1. Introduction

The modes of laterally heterogeneous, anelastic rotating, elliptical Earth models are generally

found by the variational method, in which the eigenfunctions are expanded as linear combinations of the degenerate singlets of a spherically symmetric, non-rotating, non-dissipative model; the eigenfrequencies and expansion coefficients are then found by solving a matrix eigenvalue problem. In principle, a complete (and thus infinite) basis set would lead to exact eigensolutions for a laterally heterogeneous, anelastic, rotating,

* Present address: Texas Instruments, MS 3402, P.O. Box 405, Lewisville, TX 75067, U.S.A.

** Present address: Seismological Laboratory, California Institute of Technology, Pasadena, CA 91125 U.S.A.

elliptical model; in practice, the cost, speed and memory of presently available computational facilities place an upper limit on the dimension of the usable basis set. Progress in computer technology has led to a rapid growth of this limit in the recent past, and this trend may reasonably be expected to continue.

The main topic of this paper is the computation by the variational method of eigensolutions and synthetic spectra for laterally heterogeneous, anelastic, rotating, elliptical Earth models. This yields forward model calculations that are as accurate as is now possible, and allows quantitative study of phenomena such as coupling between multiplets. Using results presented by Tsuboi et al. (1985) and by Tsuboi (1985) the variational solutions presented in this study can be used to obtain the partial derivatives of eigenfrequencies, eigenfunctions and synthetic seismograms with respect to an initially laterally heterogeneous, anelastic, rotating, elliptical Earth model.

In this study we compare results obtained by the variational method to those obtained using first order degenerate perturbation theory and quasidegenerate perturbation theory. First-order degenerate perturbation theory (e.g., Madariaga, 1972) limits the basis set to the degenerate singlets from a single unperturbed multiplet of the spherically symmetric model. Quasi-degenerate perturbation theory (e.g., Luh, 1973, 1974; Masters et al., 1983; Park, 1985) limits the basis set to two or three adjacent multiplets of the spherically symmetric model. On the basis of simple test cases, Geller and Stein (1978), Morris and Geller (1982) and Tanimoto (1982) concluded that a full variational procedure was probably required to obtain an adequate representation of the modes of a laterally heterogeneous model. However, the geometries of these cases were special, and we therefore perform numerical experiments for the more realistic models considered in this study.

2. Variational solution of anelastic problems

We represent the eigenfunction and dual space eigenfunction as linear combinations of the degenerate singlets of the spherically symmetric part of

the model. We then express the Lagrangian as a bilinear form in terms of the expansion coefficients of the eigenfunction and the dual space eigenfunction. We finally use the fact that the Lagrangian must be stationary with respect to an arbitrary infinitesimal perturbation of the eigenfunction or the dual space eigenfunction (Rayleigh's Principle) to obtain a matrix eigenvalue problem for the expansion coefficients and the eigenfrequency.

In this study we approximate the effect of anelastic attenuation by using a complex shear modulus. The potential energy matrix is therefore complex and non-hermitian. However, the above procedure (expanding the eigenfunction and dual space eigenfunction in terms of trial functions, computing the matrix elements, and then applying Rayleigh's Principle) is applicable whether or not anelasticity (or the Earth's rotation) is included in the calculation. We therefore refer to this procedure as the variational method for both the elastic and anelastic problems. On the other hand, Tanimoto (1982) and Park (1985) use the term 'Galerkin method' when this method is applied to the anelastic problem. Because the same procedure is used whether or not anelasticity is included, it seems desirable to use the term 'variational method' for both the elastic and anelastic cases. Some, but not all, texts follow this usage. For example, Finlayson (1972) calls the procedure for finding the eigenstates of a non-self-adjoint problem the 'adjoint variational method'. It should be emphasized that the variational method is a subset of the Galerkin method (e.g., Finlayson, 1972).

The term 'Galerkin method' essentially encompasses all cases in which an inhomogeneous differential equation is solved by expanding the solution in terms of basis functions. This procedure can be used whether or not the corresponding homogeneous equation has any non-trivial solutions (i.e., eigensolutions). For example, the wave equation for a one-dimensional homogeneous string with a fixed boundary at $x = 0$ has homogeneous solutions of the form $u = \sin kx$. If such a string has a radiation boundary condition, $u' + iku = 0$, at its right-hand end, it is easy to see that there are no non-trivial homogeneous solutions

(e.g., Geller et al., 1985). Thus the inhomogeneous problem cannot be solved by an eigenfunction expansion, because there are no modes. On the other hand, the inhomogeneous problem can be solved by directly expanding the solution in terms of some set of orthogonal functions, and solving for their coefficients. This method of solution has in fact been implemented by Spudich and Ascher (1983) for seismic body wave problems in a halfspace with a free surface and a radiation condition at depth, and is an example of the more general Galerkin method (or collocation method).

A string (or halfspace) with one free (or fixed) and one radiation boundary condition is a physically unrealizable system, and has no non-trivial homogeneous solutions. In contrast, the anelastic systems we consider have sets of non-trivial homogeneous solutions (modes) that span the space of possible motion*. These modes are stationary states of the Lagrangian, just as are the modes of a perfectly elastic system. We therefore use the term 'variational method' to describe the procedure used in this study for calculating the modes of a laterally heterogeneous, anelastic, rotating, elliptical model.

3. Theory, basis selection, and the eigenvalue problem

We seek linear combinations of the basis functions which closely approximate the left (dual space) and right (receiver space) eigenfunctions of a laterally heterogeneous, rotating, anelastic model. As in Morris and Geller (1982), the normal modes of a laterally homogeneous, spherically symmetric, non-rotating model are used as the basis, and linear combinations of these functions are found which make the Lagrangian of the laterally heterogeneous model stationary. The details of this procedure are given elsewhere (Morris and Geller, 1982; Morris, 1985) so only a brief discussion is given here.

* This is true even if the anelastic system is defective. This can be seen by considering a critically damped harmonic oscillator with one degree of freedom, whose modes are $\exp(-\omega_0 t)$ and $t \exp(-\omega_0 t)$. The defective modes (if any) of a system with multiple degrees of freedom exhibit the same behavior.

The ket $|k\rangle$ represents a basis toroidal or spheroidal eigenfunction of overtone n , angular order l , and azimuthal order m . The ket $|v\rangle$ and the bra $\langle u|$ are, respectively, an eigenfunction of the laterally heterogeneous model and the corresponding dual space eigenfunction

$$|v\rangle = \sum_k C_k |k\rangle \quad |k\rangle = |n, l, m\rangle \quad (1a)$$

$$\langle u| = \sum_k D_k \langle k| \quad \langle k| = \langle n, l, m| \quad (1b)$$

C_k and D_k are unknown expansion coefficients that will be found by solving the matrix eigenvalue problem. There is no simple relation between C_k and D_k for an anelastic, rotating model. Substituting the expansions for $\langle u|$ and $|v\rangle$ into the Lagrangian and taking the variation with respect to \mathbf{D} gives the matrix eigenvalue problem

$$(\omega^2 \mathbf{T} - \omega \mathbf{R} - \mathbf{V})\mathbf{C} = 0 \quad (2)$$

where \mathbf{T} is the matrix of kinetic energy terms, \mathbf{V} is the matrix of potential energy terms (including anelasticity), \mathbf{R} is the matrix of terms related to the Coriolis force, and the elements of \mathbf{C} are the coefficients C_k from (1). If we had taken the variation with respect to \mathbf{C} instead, we would have obtained the matrix eigenvalue problem for the left (dual space) eigenfunction's expansion coefficients in place of (2). The elements of \mathbf{T} and \mathbf{V} are

$$\mathbf{T}_{k'k} = \langle k' | \rho(r, \theta, \phi) | k \rangle \quad (3)$$

and

$$\mathbf{V}_{k'k} = \langle k' | \mathbf{E}(r, \theta, \phi) | k \rangle \quad (4)$$

where ρ is the density operator, and \mathbf{E} contains the strain, gravitational, and rotational potential energy operators. The strain energy operator includes both elastic and anelastic terms.

For any solution to (2), first-order degenerate perturbation theory restricts the sum in (1a) and (1b) to the $2l+1$ degenerate singlets within a single unperturbed multiplet. The solutions for ${}_0S_{32}$, for example, would consist of linear combinations of only the 65 singlets of the degenerate multiplet. In contrast the basis for the variational

procedure includes not only these 65 singlets, but also as many other singlets as is numerically feasible.

Selection of the most appropriate basis for a given set of computations is an important problem. Unfortunately, there is no clear method of determining a priori which trial functions must be included in the basis. Some effects can be predicted by using the selection rules. For example, it is well known that the Coriolis force and ellipticity create coupling between toroidal and spheroidal modes with angular orders differing by one: (${}_n S_l - {}_n T_{l\pm 1}$), and between toroidal modes or spheroidal modes whose angular orders differ by two: (${}_n S_l - {}_{n'} S_{l\pm 2}$ and ${}_n T_l - {}_{n'} T_{l\pm 2}$). Based on some quasi-degenerate computations, Luh (1974) and Masters et al. (1983) suggested that toroidal-spheroidal Coriolis coupling is the single most important effect in the frequency band below about 3 mHz, but that aspherical structure becomes more important above those frequencies.

Unfortunately, as the effect of the lateral heterogeneity increases, the selection rules become progressively less accurate in predicting which trial functions will significantly contribute to any particular eigenfunction. In some cases (e.g., Geller and Stein, 1978, fig. 2) strong coupling may occur even though the corresponding matrix element is zero. The results of the variational calculation are most important for those cases in which such strong coupling occurs.

It appears that rules of thumb based on the selection rules and the magnitude of the matrix elements apply to calculations presented in this study. However, the adequacy of the present basis set must ultimately be confirmed by numerical tests using a much larger set of which the present basis is a subset. Extensive computational experiments should be performed regarding this important question.

4. Solution of the eigenvalue problem

The derivation of the matrix elements is discussed in detail elsewhere (Madariaga, 1972; Luh, 1973, 1974; Woodhouse and Dahlen, 1978; Woodhouse, 1980) and will not be repeated here.

The matrix elements are summarized in the Appendix. Note that a minor error in the ellipticity terms of Woodhouse (1980) is corrected.

Equation 2 contains both terms in ω and ω^2 , so solving it directly would double the order of the eigenvalue problem (Lancaster, 1966; Garbow et al., 1977). (The term that is linear in ω is due to Coriolis forces.) To eliminate the ω term, after Woodhouse (1980) and Masters et al. (1983), the matrix elements in (2) are approximated by

$$\omega R_{k'k} = (\omega_{k'} \omega_k)^{1/2} R_{k'k}$$

where, ω_k is the unperturbed frequency of the basis singlet $|k\rangle$. This approximation allows the Coriolis terms to be combined with the potential energy terms, and reduces (2) to the more manageable form

$$\omega^2 TC = V' C \quad (5)$$

where V' is the sum of V and the Coriolis terms.

The eigenvalue problem in (5) was solved using a program and algorithm similar to those in EISPACK (Garbow et al., 1977). This method simultaneously reduces the matrices on both sides of (5), and then iterates on successively smaller matrices to isolate the eigenvalues; $O(N^3)$ operations are required to compute all N eigenvalue/eigenvector pairs.

The eigenvalue problems were solved using the Hitachi S-810/20 supercomputer at the Computer Centre of the University of Tokyo. This supercomputer system has a maximum speed of about 800 MFLOPS and 64 Mbytes of physical memory (128 MB as of July 5, 1986). At the time we made these calculations, it did not have virtual memory and we could use a maximum of 16 Mbytes for one process. Therefore we could solve a 351×351 problem in core quite easily. A total of 30 s of CPU time (of which 15 s were used by the VPU—attached Vector Processing Unit) was required to solve a single 351×351 problem on the HITAC S-810/20 supercomputer. The cost was about US\$2.50 at the then prevailing exchange rate. 10 CPU min were required to solve the same problem on the Hitachi M-280H, a standard mainframe system. The size of the basis set likely to be required in the future will be at least 700–1000; therefore the use of a supercomputer is

essential for this problem. Before using the Hitachi supercomputer, a VAX 11/780 at Stanford University was used for this calculation. It took about 10 CPU h to solve the same problem on the VAX 11/780. It is true that the amount of time required to solve the problem was not only dependent upon processor speed, but was also strongly related to the amount of memory on the machine used. However, it is obvious that both speed and memory requirements for this relatively small problem already exceed the limits of the 'super-mini' class of computers.

At the time this work was performed, the largest problem that could be run on the Hitachi was about 700×700 because of memory limitations. It took 25 min 34 s of CPU time to solve this problem, of which about 7 min was VPU time. For this case, the matrix elements could be stored in core but to obtain the eigenvectors, it was necessary to use disk I/O. Therefore about 90% of the CPU time was used for disk I/O rather than computation. It is instructive to examine the computer resources required by a problem of this size. Table I summarizes the performance of the algorithm on four different machines for a basis size of 351.

TABLE I

Summary of computer resources required to solve $\omega^2 TC = V'C$ for a basis of 351 singlets

Computer	Physical memory	Average memory available to process	CPU time required
Hitachi S810 (Tokyo University)	64 Mbytes	16 Mbytes	~ 30 s
VAX 11/780 (Stanford University)	8 Mbytes	4.5 Mbytes	~ 800 min
VAX 11/750 (Stanford University)	6 Mbytes	3.0 Mbytes	~ 1200 min
VAX 11/750 (Stanford University)	2 Mbytes	0.8 Mbytes	> 2000 min

The total memory required by the process was about 5.8 Mbytes. When the problem was run on the two-megabyte VAX 11/750, it was less than half finished when a system crash killed it at 2000 CPU min.

5. Laterally heterogeneous models

In subsequent sections we present eigenvibration computations for three models of the Earth's lateral heterogeneity (Figs. 1 and 2):

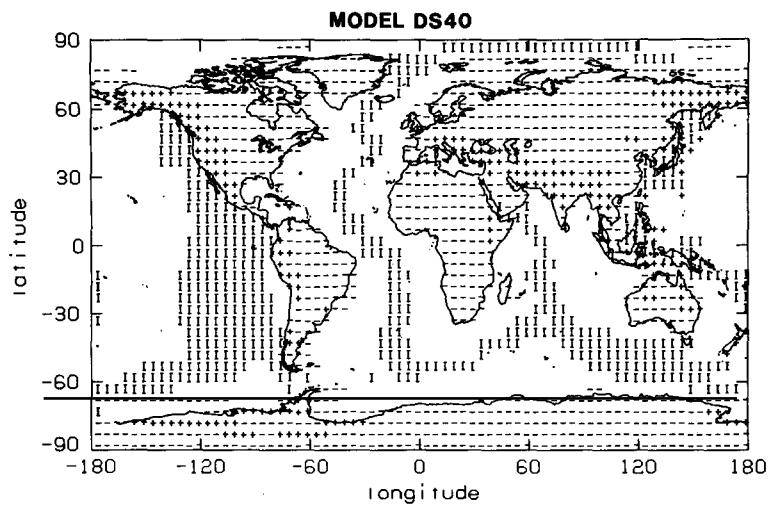
(1) a slight modification of a regionalized model of lateral heterogeneity proposed by Dziewonski and Steim (1982), in which lateral heterogeneity extends to a depth of 670 km.

(2) A model that has the same properties as (1) at depths shallower than 216 km, but which is laterally homogeneous below that depth.

(3) A model that carries lateral heterogeneity to a depth of 216 km and uses Okal's (1977) surface regionalization. The oceanic areas are subdivided into four regions, classified according to age.

The surface regionalization of each of the three models is expanded up to angular order $s = 40$ (a surface wavelength of about 1000 km). Including such high order lateral heterogeneity can significantly affect the computed coupling and splitting. However, the selection rules require that laterally heterogeneous structure with angular order $s \leq l + l'$ must be included in calculating the matrix element for coupling between the trial functions from the l th and l' th multiplets. Thus, for example, laterally heterogeneous structure up to angular order $s = 63$ will affect the matrix element for coupling between ${}_0T_{31}$ and ${}_0S_{32}$. Therefore, if there are such sharp discontinuities in the lateral structure of the actual Earth (e.g., the ocean-continent boundary) they must be included in the computations. Further work is required to determine what proportion of the splitting and coupling found in this study is due to the higher angular order portion of the above models. In the future, it should be possible to determine, by comparing the results of the variational calculations to observations, the extent of the Earth's short wavelength laterally heterogeneous structure.

The first model, DS40 (Fig. 1), is based on the Dziewonski and Steim (1982) regionalized model of lateral variations in V_s in the upper mantle. This model, which was obtained from surface wave data, contains three zones of lateral heterogeneity between the depths of 80 and 670 km, and uses a surface regionalization which defines four regions: continent, young ocean, old ocean, and



Young Ocean: I
 Old Ocean: -
 Stable Continents: +
 Tectonic Regions: -

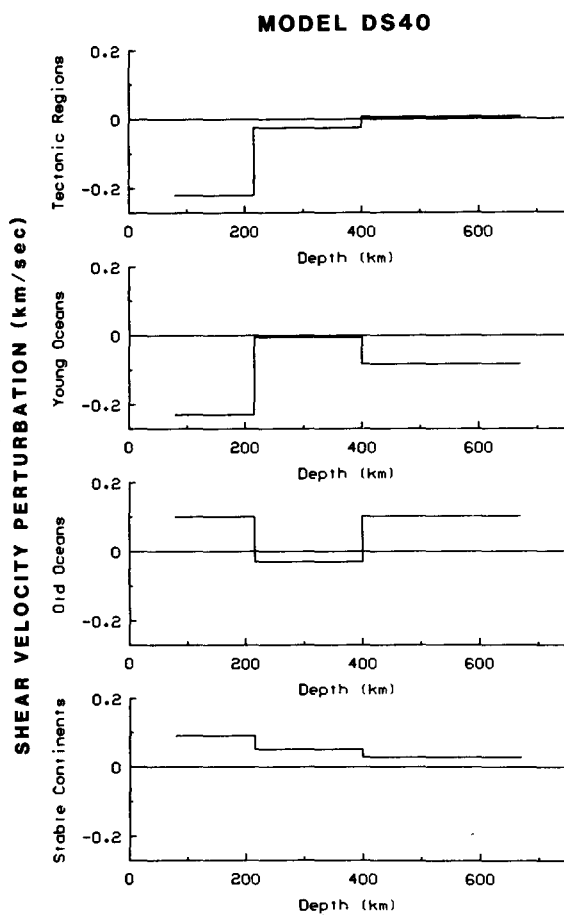


Fig. 1. (a, top) Surface regionalization for Dziewonski and Steins' (1982) model of lateral heterogeneity (model DS40 in this study). This regionalization is also used for model TR40. (b, bottom) Perturbations to shear velocity as a function of depth for models DS40 and TR40. The perturbations between 80 and 670 km are those proposed by Dziewonski and Steins (1982) for model DS40; model DS40 has simply been truncated below 216 km to form model TR40. The perturbations in density and compressional velocity were scaled to the shear velocity perturbations in the manner suggested by Masters et al. (1982): $d(\ln \delta\rho)/d(\ln \delta V_s) = 0.4$ and $d(\ln \delta V_p)/d(\ln \delta V_s) = 0.8$.

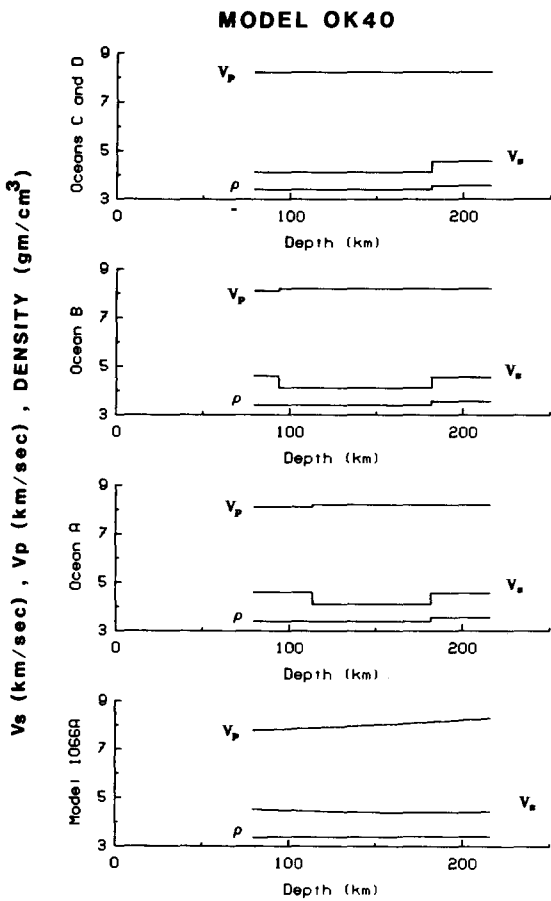
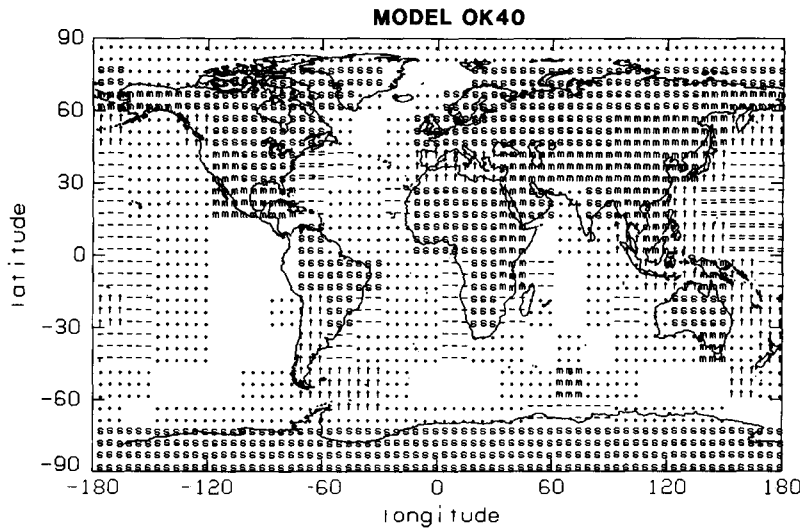


Fig. 2. (a, top) Okal's (1977) surface regionalizations, which form the basis for model OK40. Okal's regions 't' and 'm' have been combined into a single region, underneath which the shear velocity perturbations are the same as for the upper 216 km of region 't' in model DS40. (b, bottom) Shear velocity, compressional velocity, and density as a function of depth under the oceanic regions of OK40. After Okal (1977), region 'A' (plotted as '=') is the same as Leeds' (1975) Ocean 1, region 'B' (plotted as '-') averages Leeds' Oceans 2 and 3, region 'C' ('.') averages Leeds' Oceans 3-6, and region 'D' (blank) averages Oceans 6-8. Regions 'C' and 'D' are identical in this experiment, since they differ only at depths shallower than 77 km, and the zones of lateral heterogeneity used in this experiment did not extend to such a shallow depth.

tectonically active. Perturbations to compressional velocity and density were scaled to the perturbations in V_s using the method described by Masters et al. (1982), and the corresponding perturbations to shear modulus and bulk modulus were computed from these values using the scaling laws ($d(\ln \delta\rho)/d(\ln \delta V_s) = 0.4$ and $(d(\ln \delta V_p)/d(\ln \delta V_s) = 0.8)$). The second model, TR40, is identical to model DS40 to a depth of 216 km, but contains no lateral heterogeneity below that depth.

The third model, OK40 (Fig. 2), uses Okal's (1977) surface regionalization, which defines shield, Phanerozoic mountain, and trench/marginal sea regions, and which breaks up the oceanic regions into four zones, based on combinations of the eight age classifications of Leeds (1975). Okal's region A corresponds to Leeds' Ocean 1, region B is an average of Leeds' Oceans 2 and 3, region C averages Oceans 3–6, and region D is an average of Oceans 6–8. The variations of shear velocity, compressional velocity, and density with depth under each of Okal's oceanic regions were obtained by averaging the appropriate Leeds ocean models (Fig. 2a). Since Okal did not specify the properties under the continental or trench/marginal sea portions of his models, the same values were used for those areas as for the DS40 model. The Phanerozoic mountain and trench/marginal sea regions were combined into one 'tectonic' region for this purpose. (Although it would have been slightly better to match some of the trench/marginal sea regions to Dziewonski and Steim's (1982) young oceanic crust, the shear velocity perturbations under the young oceanic and tectonic regions of the Dziewonski and Steim model are very nearly the same above 200 km.) Also, in order that the depth range of lateral heterogeneity would be the same for model OK40 as for model TR40, the model contains no lateral variations shallower than 80 km. This effectively combined Okal's regions C and D, since they do not differ below 80 km.

Masters et al. (1982) cautioned that eigensolutions were sensitive to the choice of the scaling of lateral variations in compressional velocity and density to the shear velocity perturbations. Our primary interest in this study is to make comparisons between the models, and between the varia-

tional method and first order degenerate perturbation theory. However, this question clearly requires further study in the future. With the exception of the oceanic regions in model OK40, the models were scaled in the same way, so the choice of scaling should not affect comparison between the eigensolutions for models DS40 and TR40. In addition, the main interest in comparing model OK40 with the others is to examine the effect of varying the properties shallower than 200 km under oceanic regions; thus, the fact that OK40 is scaled somewhat differently under its oceanic regions is of minor importance.

6. Reference model and basis set

The spherically symmetric reference model for this experiment was taken to be model 1066A of Gilbert and Dziewonski (1975). To make the spherical harmonic expansions of the perturbations consistent with this choice, we set the Y_0^0 ($s = 0, t = 0$) components of the model parameter expansions to zero. Spherically symmetric attenuation (Fig. 3a) was incorporated in models DS40, OK40, and TR40 by applying the Q^{-1} model of Stein et al. (1981) to the shear modulus distribution of model 1066A, $\mu_0(r)$, and constructing a spherically symmetric imaginary part of the shear modulus (Fig. 3b), $\mu_0^{im}(r) = \mu_0(r)Q^{-1}(r)$. For simplicity, we chose not to consider laterally heterogeneous anelasticity; however, if desired, it could easily be included in the calculations.

The basis set for the computations consists of the degenerate singlets of 7 spheroidal and 4 toroidal degenerate multiplets of model 1066A, for a total of 351 singlets (Table II), encompassing a frequency band of 3.943 to 4.035 mHz. This choice of basis gave a set of modes that: (1) were of high enough frequency to be affected by the zones of heterogeneity in the models, (2) formed an eigenvalue problem of manageable size without all the modes involved being effectively degenerate, and (3) allowed fundamental-overtone coupling to be examined in a region of the spectrum where fundamental mode Coriolis coupling (between ${}_0T_{31}$ and ${}_0S_{32}$) is important.

The depth-dependent part of the eigenfunctions

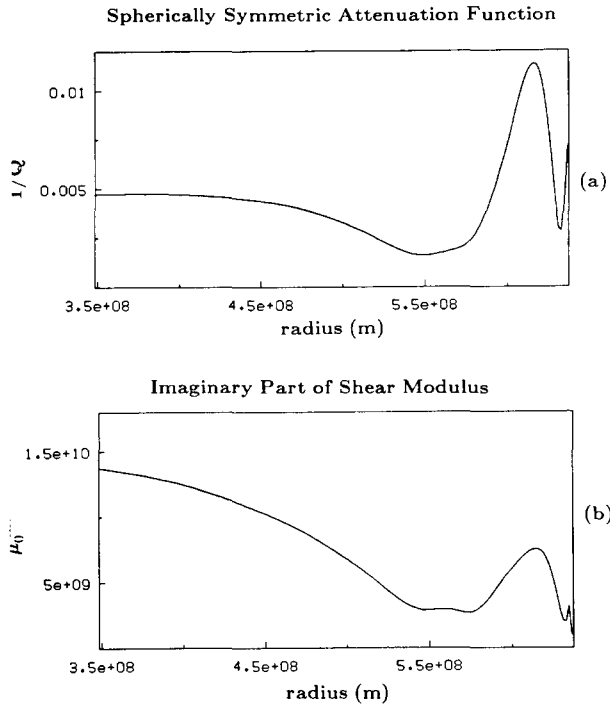


Fig. 3. (a) Spherically symmetric Q^{-1} model of Stein et al (1981) applied to models DS40, TR40, and OK40. (b) The complex part of the spherically symmetric shear modulus resulting from $\mu_0^i(r) = \mu_0^e(r)/Q(r)$.

for all the degenerate multiplets in the basis was expressed as a series of cubic polynomials, after Wiggins (1976). The spheroidal modes were taken

TABLE II

Unperturbed multiplets of model 1066A which formed the basis set for the computations in this study

Basis multiplet	Frequency	
	(rad s^{-1})	(mHz)
${}_0T_{31}$	2.5096385e-02	3.9942137e+00
${}_1T_{19}$	2.5172060e-02	4.0062578e+00
${}_2T_{14}$	2.5242394e-02	4.0174518e+00
${}_3T_{10}$	2.5106283e-02	3.9957890e+00
${}_0S_{32}$	2.5086936e-02	3.9927099e+00
${}_1S_{20}$	2.4771513e-02	3.9425087e+00
${}_3S_{16}$	2.4921826e-02	3.9664318e+00
${}_4S_{11}$	2.5199956e-02	4.0106976e+00
${}_6S_9$	2.4886725e-02	3.9608453e+00
${}_7S_6$	2.4855318e-02	3.9558467e+00
${}_{10}S_2$	2.5350178e-02	4.0346061e+00

from a set of modes computed for model 1066A by Buland (1976), and the toroidal modes were computed by similar programs written locally (R. Haar, personal communication, 1982).

7. Eigenfrequencies

Our primary interest is to determine the nature of singlet splitting caused by laterally heterogeneous structure. However, we begin by considering the splitting in a model including anelasticity, rotation and ellipticity, without including any lateral heterogeneity. First we calculate the splitting due to rotation and anelasticity alone (Fig. 4). The horizontal axis of Fig. 4 is the real part of the eigenfrequency in mHz, and the vertical axis is $Q^{-1} = 2 \text{Im}(\omega_k)/\text{Re}(\omega_k)$. We can see that the effect of rotation does not in general cause sizable splitting of eigenfrequencies in this frequency range. However, the Coriolis coupling between ${}_0T_{31}$ and ${}_0S_{32}$ is significant.

Next we include rotation, ellipticity and attenuation in (2). Figure 5 is a plot of the eigenfrequencies for this case. The width of splitting becomes larger because of ellipticity, but the coupling between multiplets is significant only for ${}_0T_{31}$ and ${}_0S_{32}$. The results of our calculation show the importance of the ellipticity contribution, in accord with previous studies.

We then show results that include the effect of lateral heterogeneity. Figure 6a shows the eigenfrequencies for model DS40. We also include the effect of rotation, ellipticity, and attenuation. The horizontal axis and the vertical axis are the same as in Fig. 4. The variational frequencies are plotted as '+' signs. Figure 6b is a reference plot for the same model, showing the positions of the first order perturbation theory solutions for the various basis multiplets. If first order perturbation theory was sufficiently accurate (i.e., if the coupling between multiplets was negligible), the '+' signs in both figures would coincide. Instead, Fig. 6a shows that most of the first order perturbation theory solutions for model DS40 are seriously in error. For example, the error in Q^{-1} is 30% or more in many cases. This is especially significant since, for this basis set, the matrix elements af-

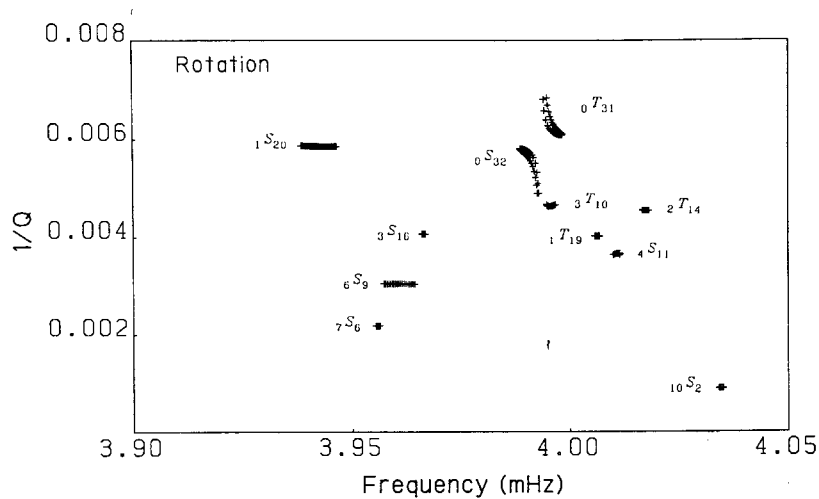


Fig. 4. Eigenfrequencies for rotational splitting (including Coriolis coupling) for an otherwise laterally homogeneous, spherical model. The spherically symmetric Q^{-1} model shown in Fig. 3 is included. The real part of the frequency is plotted as horizontal axis. The vertical axis is $Q^{-1} = 2\omega_k^m/\omega_k^e$.

ected by anelasticity were confined to the diagonal. The differences in Q^{-1} for the two sets of solutions are thus entirely due to coupling between multiplets that is omitted by first order degenerate perturbation theory. It is difficult to determine the magnitude of error in the real parts of the eigenfrequencies, since an exact correspon-

dence between singlets in the two sets of solutions cannot be determined, but it is clear that there are significant differences.

We have also calculated the modes of a model including only lateral heterogeneity and attenuation (Fig. 7a) and including ellipticity, lateral heterogeneity and attenuation (Fig. 7b). Figure 7a

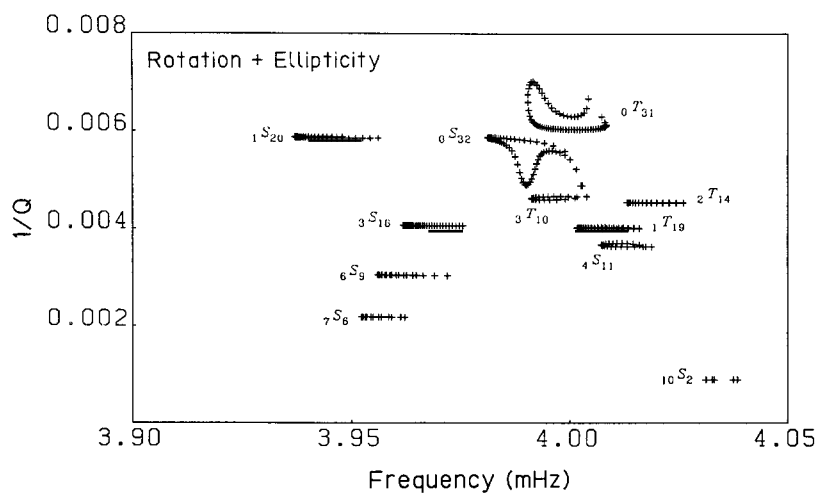


Fig. 5. Eigenfrequencies for rotational and ellipticity splitting (including Coriolis coupling) for an otherwise laterally homogeneous model. Attenuation as shown in Fig. 3 is included. Horizontal and vertical axes are the same as Fig. 4.

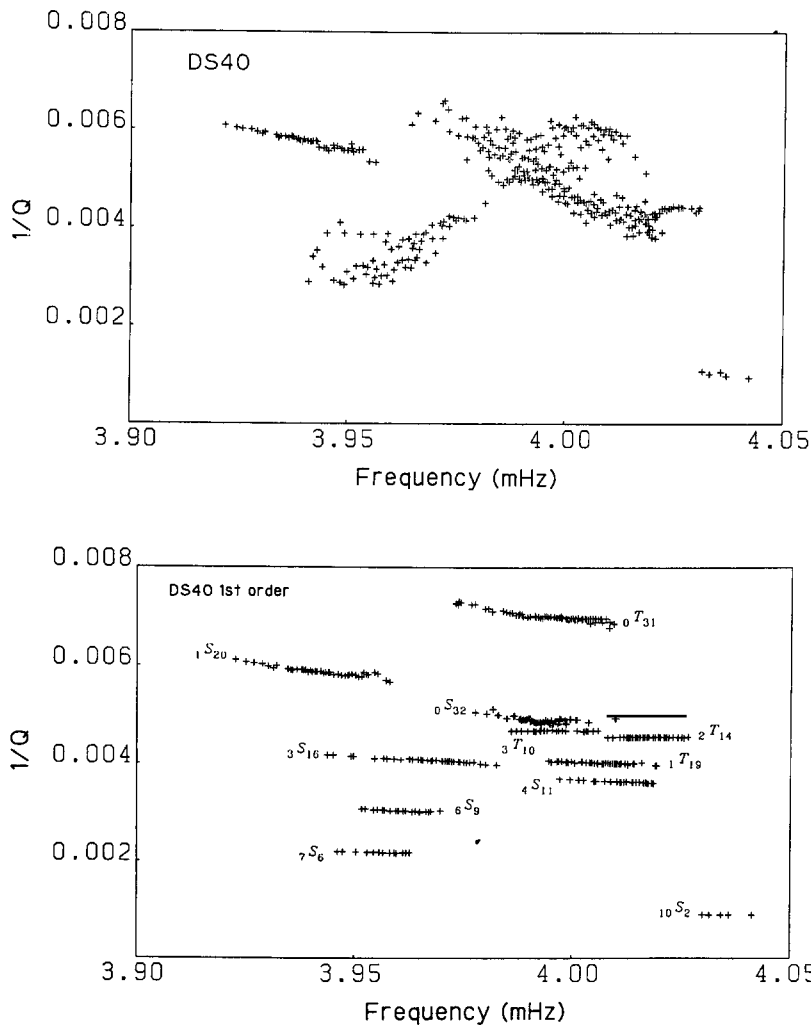


Fig. 6. (a, top) Eigenfrequencies for models DS40 as calculated by the variational method and by first order degenerate perturbation theory. Rotation, ellipticity and attenuation are also included. The horizontal axis and the vertical axis are the same as Fig. 4. The variational solutions are plotted as '+' signs. (b, bottom) Only the first-order degenerate perturbation theory solutions are plotted and labeled, as reference points for part (a).

shows that the splitting of eigenfrequencies of the modes for model DS40 is of almost the same order as that due to ellipticity (Fig. 5), however, the coupling of the modes is not large. The degree of coupling will be discussed later based on the computed eigenfunctions. By comparing Fig. 7b with Fig. 6a we can see that the effect of rotation is not negligible, even for this frequency range.

Figures 8 and 9 contain similar plots for models TR40 and OK40. The discrepancy between the first-order and variational solutions is smaller for these models than for DS40, but this is expected, since model DS40 contains much more extensive lateral heterogeneity. Again, the plots show that the Q^{-1} of the first order degenerate perturbation theory solutions is frequently seriously in error.

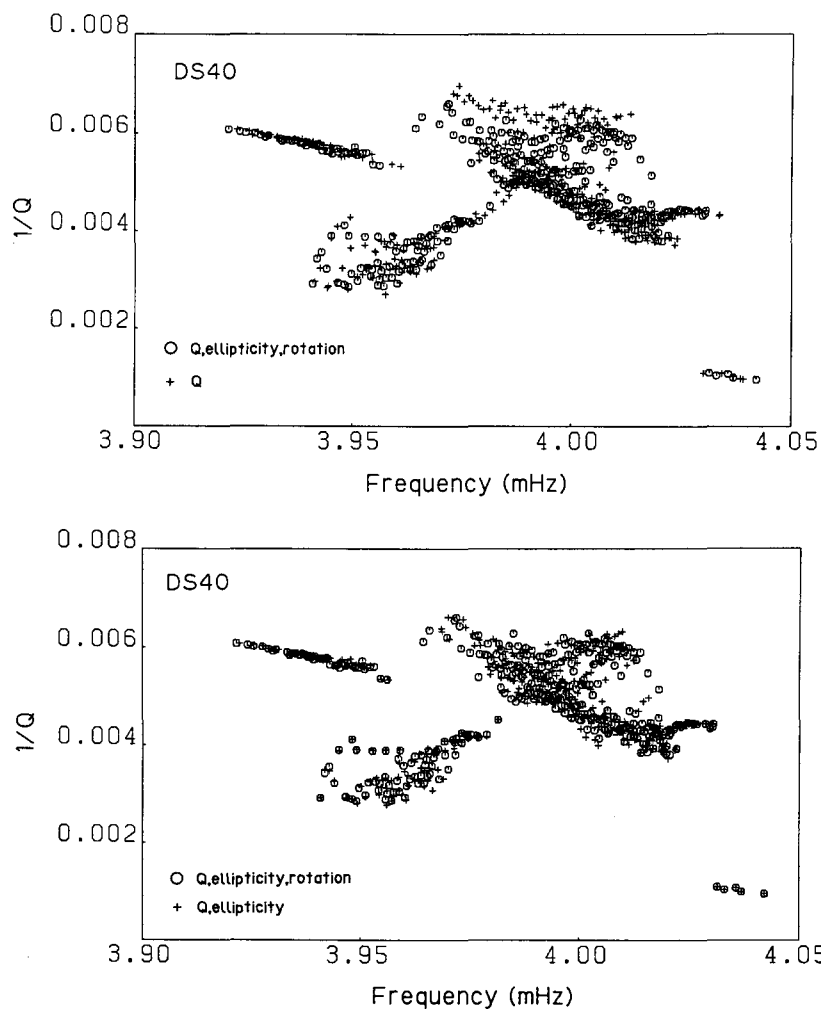


Fig. 7. Eigenfrequencies for models DS40. The horizontal axis and the vertical axis are the same as Fig. 4. (a, top) '+' are the eigenfrequencies for model DS40 (only attenuation is added). (b, bottom) The eigenfrequencies for model DS40 (rotation and ellipticity are added), which can be compared to Fig. 6a.

8. Eigenfunctions

Each eigenvector found by the variational method is specified by its 351 complex expansion coefficients. To display this information in a meaningful way, we present two types of plots in Figs. 10–12. We arbitrarily picked two singlets for each of the three laterally heterogeneous Earth models: those having the 70th and 225th smallest (real) eigenfrequencies. (Many more examples of these plots are given by Morris, 1985.) Note that

as the modes have different eigenfunctions, direct comparison of the results for different models is not meaningful. In the first type of plot (the upper part of each figure) we show, for one singlet of the laterally heterogeneous model, the total power of the expansion coefficients from each of the 11 multiplets. In the upper part of these figures we plot the quantity

$${}_n P_l = \left[\sum_m |{}_n C_l^m|^2 \right]^{1/2}$$

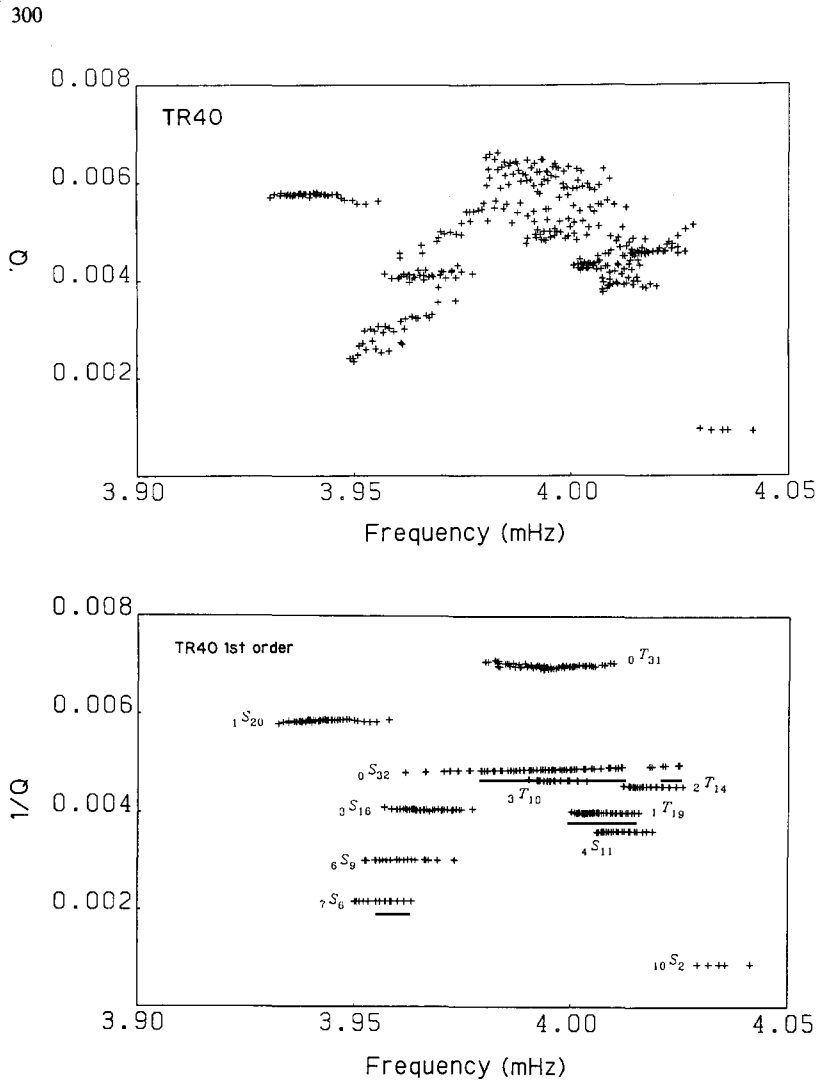


Fig. 8. Plots of the eigenfrequencies for model TR40. For further details see caption for Fig. 6.

where ${}_n C_l^m$ is the expansion coefficient of the basis singlet $|n, l, m\rangle$. The ${}_n P_l$ are plotted as sticks and are normalized so that the largest value for each solution equals 100%. To permit the spheroidal contributions to be more easily distinguished from toroidal contributions, all ${}_n P_l$ corresponding to spheroidal modes are plotted as negative, and those corresponding to toroidal modes are plotted as positive. (All of these quantities are of course positive.) Thus, these plots show the relative contribution of each basis multiplet to a particular solution.

In the second type of plot (the lower part of each figure), we show the amplitude of each of the 351 expansion coefficients for one of the singlets of the laterally heterogeneous model. The expansion coefficient ${}_n C_l^m$ refers to the degenerate singlet with angular order l , azimuthal order m (with respect to geographical coordinates) and overtone number n . Each spherical harmonic is the surface dependent part of the eigenfunction of a singlet of a laterally homogeneous, rotating model (ignoring Coriolis coupling). Thus, if rotational splitting were the dominant effect, the computed expansion

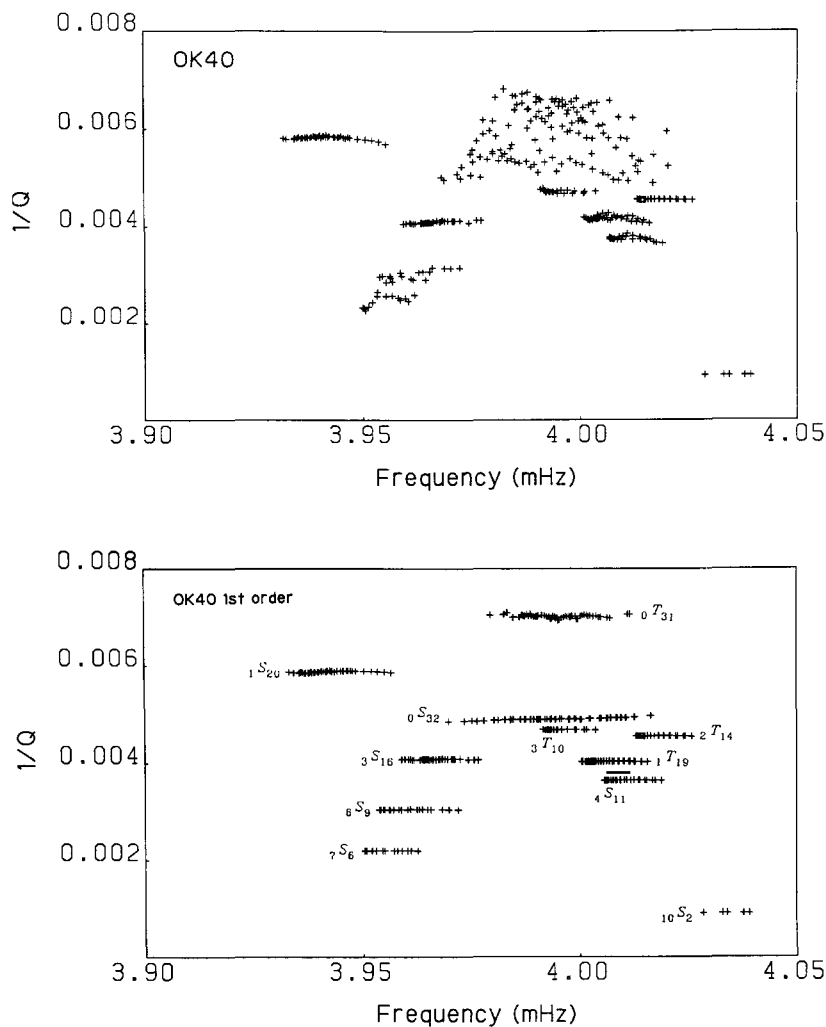


Fig. 9. Plots of the eigenfrequencies for model OK40. For further details see caption for Fig. 7.

coefficients could be regarded as physically meaningful, as lateral heterogeneity would be a minor perturbation. On the other hand, if lateral heterogeneity is as or more important than rotational splitting, then the spherical harmonic expansion coefficients have no physical meaning, regardless of the choice of coordinate system. As the latter is the case for the computations in this study, we seek a coordinate independent way of presenting the eigenfunctions computed by the variational method. While first order degenerate perturbation theory does not give sufficiently ac-

curate results, its eigenfunctions do have some physical relation to the Earth model, and are coordinate independent. We therefore present plots of the expansion coefficients of the variational solutions expressed in terms of the singlets found by first order degenerate perturbation theory.

The plot in the lower part of each figure shows the results of projecting the variational solution onto the set of eigenfunctions computed by first order degenerate perturbation theory. We use the transformation $C' = P * C$, where P is the matrix

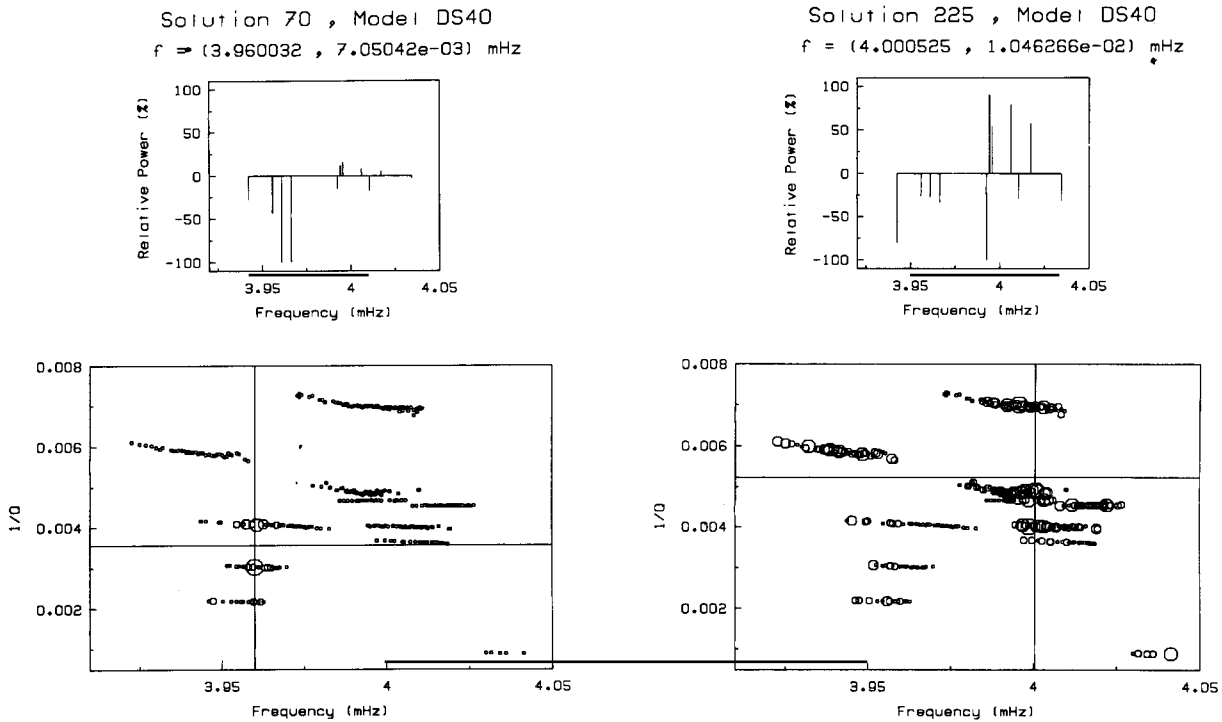


Fig. 10. (a, left) The expansion coefficients for the variational eigenfunction of the 70th mode of model DS40. (Top) The contributions to the solutions from each multiplet are summarized as a single stick, representing the total power of the expansion coefficients within each multiplet. The sticks have been normalized so that the largest is of size 100%. For convenience of display, sticks corresponding to spheroidal multiplets are plotted as negative, while sticks corresponding to toroidal multiplets are plotted as positive. (Bottom) Projection of the variational eigenvector on the first-order degeneration theory solutions. The magnitudes of the components of the projected vectors are plotted at the ω_{re} and Q^{-1} values of the corresponding first-order eigenfrequencies. The largest magnitude is normalized to size 1.0, and the different sizes of the circles group the magnitudes of the inner products at intervals of 0.2 (i.e., all inner products with sizes between 0.8 and 1.0 are plotted using the largest circle, products between 0.6 and 0.8 are plotted using the next smaller circle, and so on). (b, right) Variational eigenfunction of the 225th mode of model DS40. Details are the same as Fig. 10a.

of eigenvectors (expansion coefficients) for first order degenerate perturbation theory. The transformed vector C' is normalized so that the largest component has an absolute value of 1.0. We take advantage of another aspect of the first order degenerate perturbation theory solutions: each has an eigenfrequency (real and imaginary parts) that gives coordinates at which to plot a symbol representing the magnitude of the normalized, transformed, expansion coefficients; this is how we obtain the lower parts of Figs. 10–12. The normalized magnitudes of the elements of C' are grouped in increments of 0.2 for plotting purposes, so that

elements with magnitudes between 0.8 and 1.0 are plotted using the largest circles, elements with magnitudes between 0.6 and 0.8 are shown with the next smaller size circle, and so on.

Significant coupling between multiplets is clearly visible in all the plots. If first-order degenerate perturbation theory was approximately correct, the plots in the upper part of each figure would show one stick of magnitude 100%, and all others would be of negligible size. Instead, other multiplets in the basis set routinely contribute 20–50% as much to the solution as the multiplet for which ${}_n P_l = 100\%$. The stick plots for models

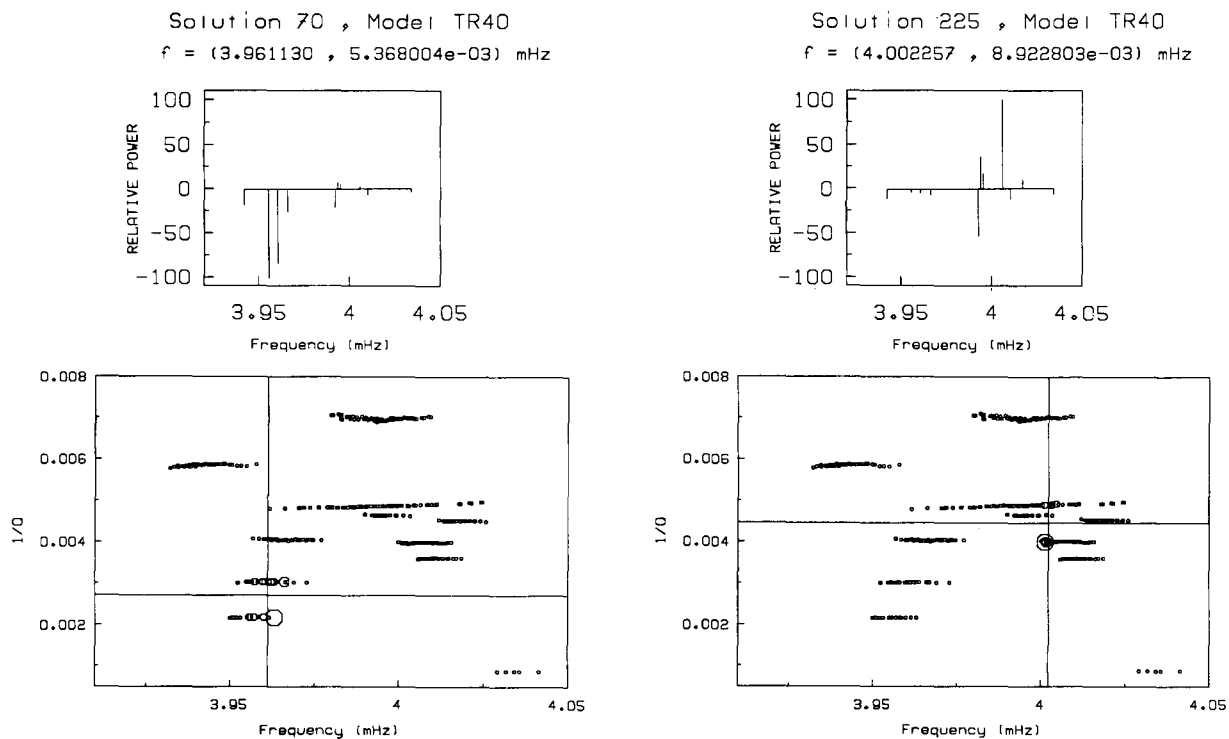


Fig. 11. (a, left) Variational eigenfunction of the 70th mode of model TR40. Details are the same as Fig. 10a. (b, right) Variational eigenfunction of the 225th mode of model TR40. Details are the same as Fig. 10a.

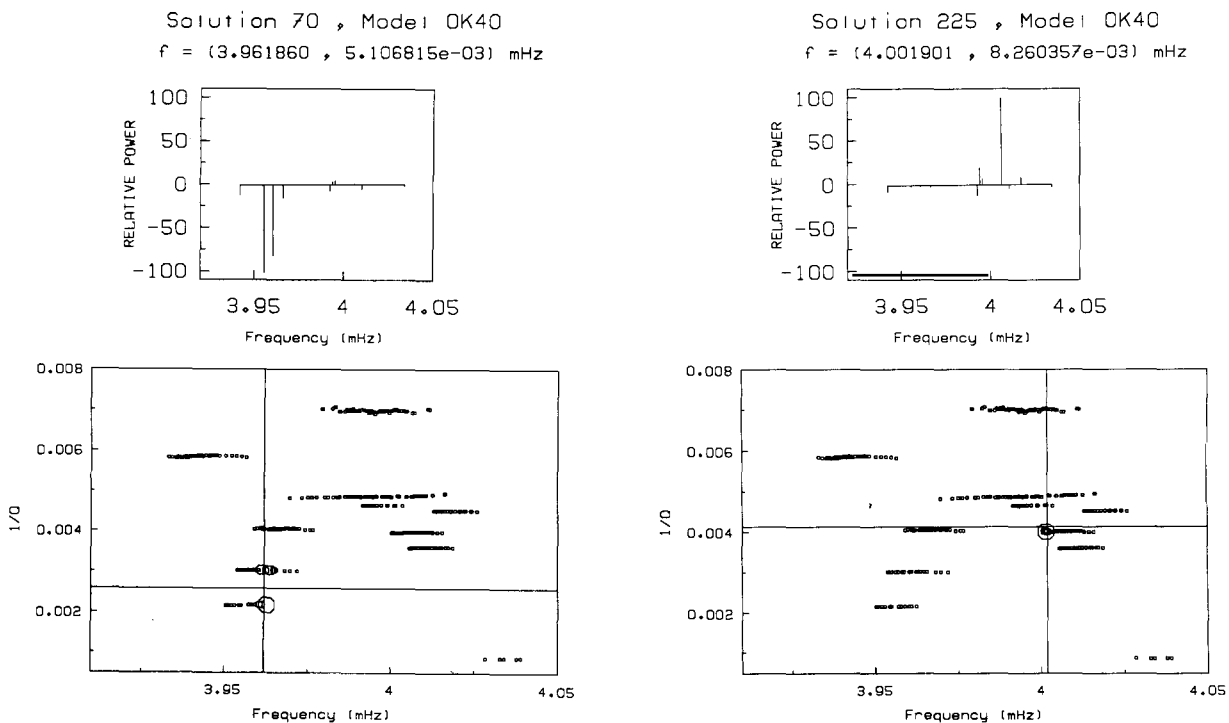


Fig. 12. (a, left) Variational eigenfunction of the 70th mode of model OK40. Details are the same as Fig. 10a. (b, right) Variational eigenfunction of the 225th mode of model OK40. Details are the same as Fig. 10a.

OK40 and TR40 show less pronounced coupling between multiplets than the figures for model DS40, but in general the coupling in the plots for these models is still not negligible. It is also interesting to look at the plots for which the largest contribution to the solution comes from either ${}_0T_{31}$ or ${}_0S_{32}$. If only fundamental mode coupling was important in these solutions, the only sticks of significant size would correspond to these two multiplets—all other ${}_nP_l$ would be negligible. This comes close to being true in some of the plots for models OK40 and TR40. However, in general, the figures show that other multiplets do significantly contribute to these cases. In fact, in Fig. 10, the contribution to the solution from ${}_1S_{20}$ is larger than the contribution from ${}_0S_{32}$.

The lower parts of Figs. 10–12 show that the largest expansion coefficients can correspond to several different degenerate multiplets. Even in cases where all sizable singlet contributions fall within one multiplet, there are generally several singlets which significantly contribute to the solution. Again, if first-order degenerate perturbation theory was substantially correct, there would be one large circle on each plot, and all the other circles would be very small. In some cases this

TABLE III

Location, magnitudes, and source mechanisms of the two events used in the computations in this study

Event	Latitude (deg.)	Longitude (deg.)	Depth (km)	m_b	M_s
1. Sumbawa, Indonesia Aug. 19, 1977 Static moment = 24.e27 Source mechanism: $\hat{m}_{rr} = -0.68$ $\hat{m}_{\theta\theta} = 0.68$ $\hat{m}_{\phi\phi} = 0.0$ $\hat{m}_{r\theta} = 0.0$ $\hat{m}_{r\phi} = -0.195$ $\hat{m}_{\theta\phi} = 0.195$	11.09S	118.46E	15	7.0	7.9
2. Honshu, Japan March 7, 1978 Static moment = .52e27 Source mechanism: $\hat{m}_{rr} = 0.489$ $\hat{m}_{\theta\theta} = 0.053$ $\hat{m}_{\phi\phi} = -0.541$ $\hat{m}_{r\theta} = 0.384$ $\hat{m}_{r\phi} = -0.551$ $\hat{m}_{\theta\phi} = -0.121$	32.00N	137.61E	439	6.9	-

All data are taken from Silver and Jordan (1983). Silver and Jordan cross-reference the source mechanisms.

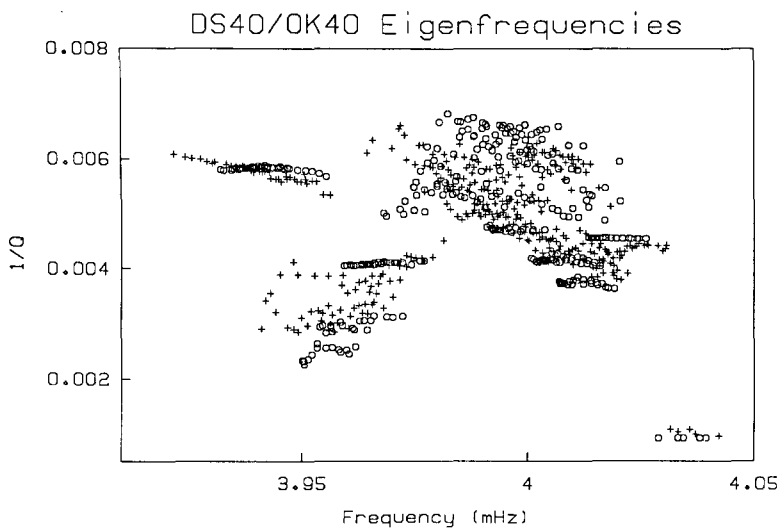


Fig. 13. (a, above) Comparison of the variational eigenfrequencies of models DS40 and TR40. The frequencies for model DS40 are plotted as '+' signs, and those for model TR40 are plotted as circles. (b, top of p. 305) Comparison of variational eigenfrequencies for models DS40 and OK40. The circles are the frequencies of model OK40 and the '+' signs represent model DS40. (c, middle of p. 305) Comparison of eigenfrequencies for models TR40 and OK40. The '+' signs correspond to model TR40; the circles correspond to model OK40.

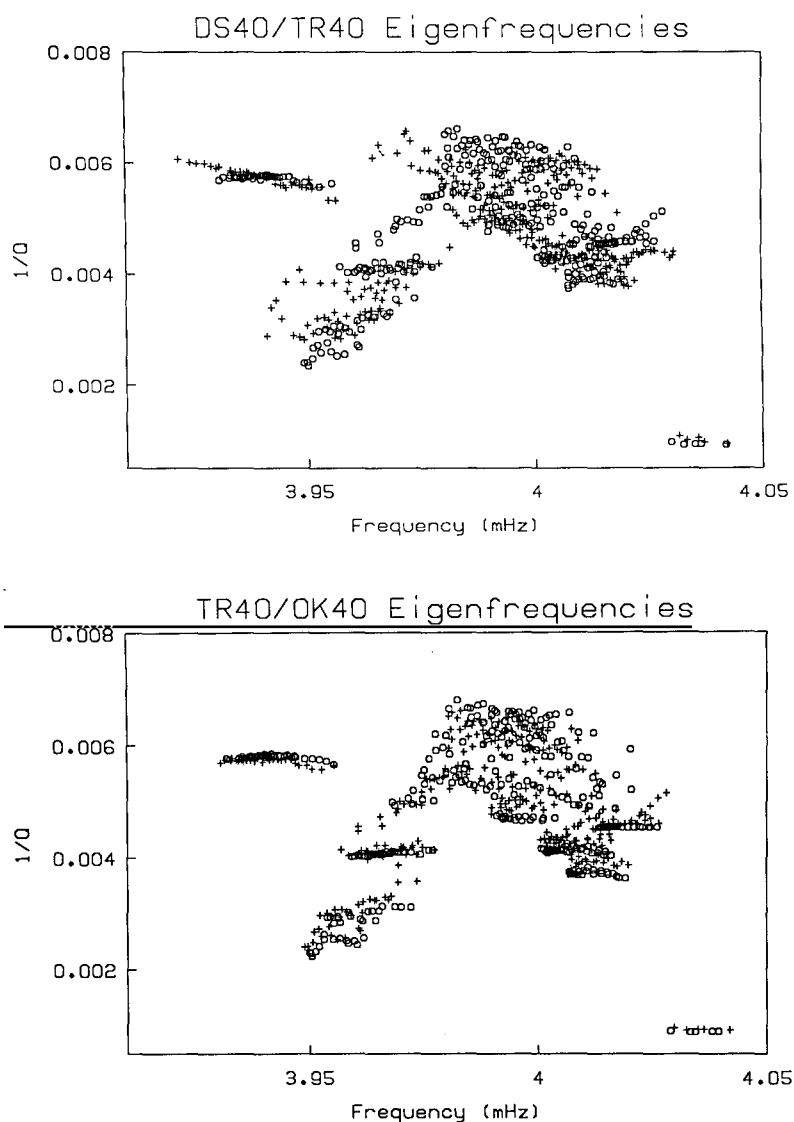


Fig. 13 (continued).

appears to happen, but in general does not.

The cross-hairs in the lower half of Figs. 10–12 show the real and imaginary parts of the eigenfrequency of the singlet whose expansion coefficients are plotted. Note that in many (although not all) cases the largest transformed expansion coefficients correspond to the singlets calculated by first order degenerate perturbation theory whose eigenfrequencies are close to the variational solution's eigenfrequency.

We have shown that there are significant differences between the results of the variational eigensolution calculations and those from first order degenerate perturbation theory. We now compare the eigenfrequencies (computed by the variational method) for the three different Earth models. Figure 13a–c show that there are potentially observable differences in the split eigenfrequencies of the three laterally heterogeneous Earth models.

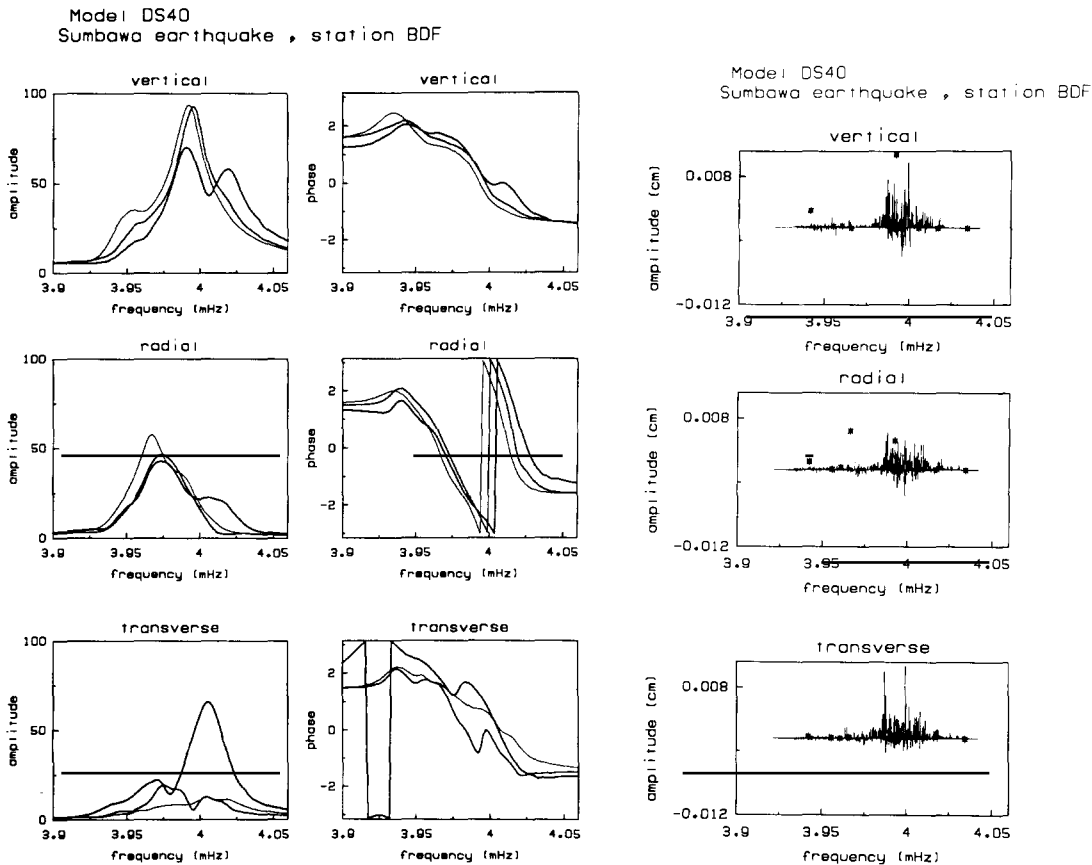


Fig. 14. (a, left) Synthetic amplitude and phase spectra at the site of the IDA station, BDF, for the mechanism of the 1977 Sumbawa earthquake, and for model DS40. Synthetic spectra for the variational solution (the thickest line), first order perturbation theory (medium thickness) and a laterally homogeneous Earth (the thinnest), are presented. The amplitude scale is in cm-s. (b, right) Absolute value of the excitation coefficients (line spectra) for the three sets of eigensolutions used to compute the synthetic spectra in Fig. 14a. The excitation coefficients for the variational method are plotted pointing upward, those for first-order degenerate perturbation theory are shown pointing downward, and the coefficients for model 1066A are shown as asterisks.

9. Synthetic spectra

Synthetic spectra for each of the three laterally heterogeneous Earth models are calculated using the eigensolutions calculated by the variational method. For comparison, we also show the spectra calculated using the first order degenerate perturbation theory eigensolutions, and those for a laterally homogeneous, nonrotating model. We present spectra for two earthquakes: the Sumbawa event of 1977, a large, shallow, normal event located seaward of the eastern end of the Java

trench and the 1978 Honshu event, a deep focus earthquake, occurring near the bottom of the seismic zone 250 km west of the Bonin Islands. Source parameters used for the synthetics are given in Table III. The depths and source mechanisms were obtained from tables 1 and 2 of Silver and Jordan (1983). These events were chosen because the earthquakes were at very different depths (15 and 439 km, respectively). All of the synthetics are calculated for a receiver at the site of the IDA station BDF, but the spectra for all three components of ground motion are given. Additional ex-

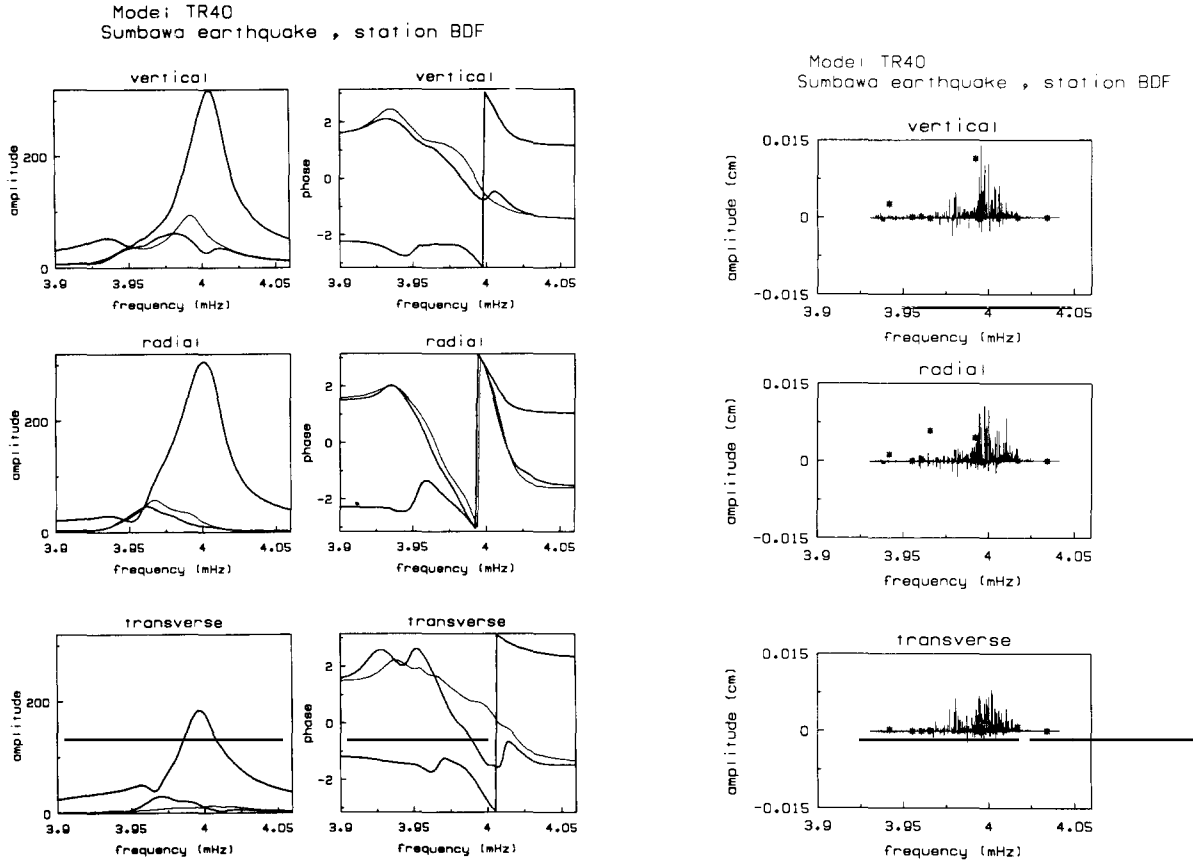


Fig. 15. (a, left) Spectra for model TR40. Other details are the same as Fig. 14a. (b, right) Line spectra for Fig. 15a. Other details are the same as Fig. 14b.

amples of these spectra are given by Morris (1985).

The eigenfrequencies and the left and right eigenfunctions for each of the three models were used in the following formulation for the excitation of the modes of a rotating, anelastic Earth (Geller and Tsuboi, 1987). In the frequency domain, the displacement, $\mathbf{w}(\mathbf{r}, \omega)$ excited by a point moment source, M_{ij} (as defined by Aki and Richards, 1980) is given by

$$\mathbf{w}(\mathbf{r}, \omega) = \sum_n \frac{[(\mathbf{u}_n(\mathbf{r}_o))_{i,j} \cdot M_{ij}] \mathbf{v}_n(\mathbf{r})}{i\omega(\omega^2 - (\sigma_n + i\alpha_n)^2)} \quad \text{for } \omega_{\text{Re}} > 0 \quad (6a)$$

and

$$\mathbf{w}(\mathbf{r}, \omega) = \sum_n \frac{[(\mathbf{u}_n^*(\mathbf{r}_o))_{i,j} \cdot M_{ij}] \mathbf{v}_n^*(\mathbf{r})}{i\omega(\omega^2 - (-\sigma_n + i\alpha_n)^2)} \quad \text{for } \omega_{\text{Re}} < 0 \quad (6b)$$

where \mathbf{u}_n is the left (dual space) eigenfunction, \mathbf{v}_n is the right eigenfunction, σ_n is the real part of the eigenfrequency, α_n is the imaginary part of the eigenfrequency, $(\mathbf{u}_n)_{i,j}$ is the derivative of the locally cartesian i component of displacement with respect to the j -th locally cartesian derivative, and summation over i and j is implied.

In this study only frequency domain excitation calculations are presented. However, results are also presented that could easily be used to calculate excitation in the time domain. To give the complete excitation formula in the time domain, following Geller and Tsuboi, we first define intermediate terms for the amplitude and phase of each mode at each point.

$$B_n(\mathbf{r}) \exp(i\epsilon_n(\mathbf{r})) = \frac{[(\mathbf{u}_n(\mathbf{r}_o))_{i,j} \cdot M_{ij}] \mathbf{v}_n(\mathbf{r})}{(\sigma_n + i\alpha_n)^2} \quad (7)$$

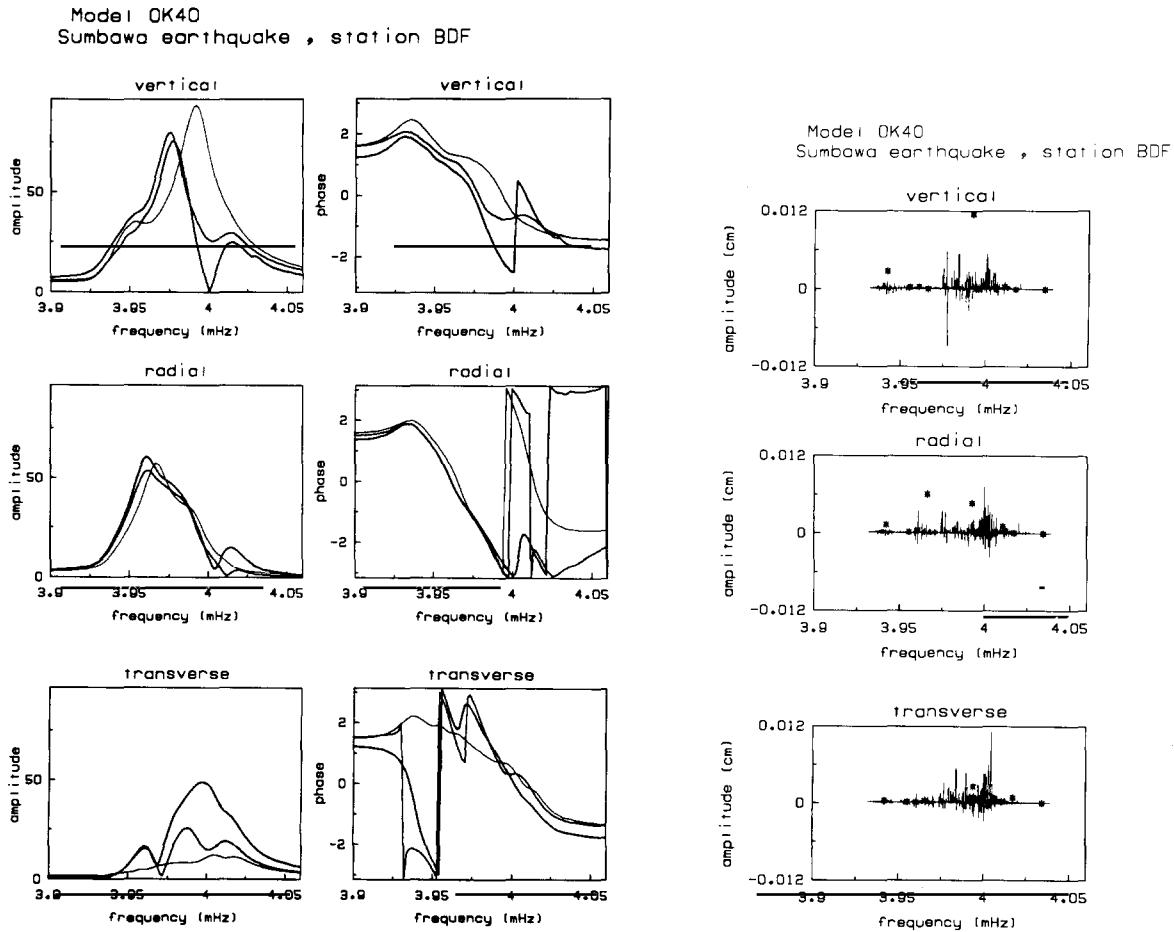


Fig. 16. (a, left) Spectra for model OK40. Other details are the same as Fig. 14a. (b, right) Line spectra for Fig. 16a. Other details are the same as Fig. 14b.

The displacement excited by a point moment tensor is then given by

$$\mathbf{w}(\mathbf{r}, t) = \sum_n B_n(\mathbf{r}) [(\cos(\sigma_n t + \epsilon_n(\mathbf{r})) \cdot \exp(-\alpha_n t)) - \cos(\epsilon_n(\mathbf{r}))] \quad (8)$$

The excitation coefficients $B_n(\mathbf{r})$ could be used in a straightforward fashion to compute synthetic seismograms if they are desired.

Figures 14–19 show synthetic amplitude and phase spectra and excitation coefficients computed at BDF. The heaviest line in each spectral plot is the synthetic obtained from the variational solution, the medium line corresponds to the

first-order degenerate perturbation theory solution, and the lightest line is the synthetic obtained from the modes of the spherically symmetric model 1066A. In the excitation coefficient plots, the coefficients for first-order perturbation theory are plotted as negative, those for the variational procedure are plotted as positive sticks, and those for model 1066A are plotted as asterisks. The line spectra for the variational, first order perturbation theory, and spherically symmetric synthetics differ greatly from one another. The errors in the synthetics calculated by the two less accurate methods generally seem to be worse for the Honshu synthetics than for the Sumbawa synthetics. This

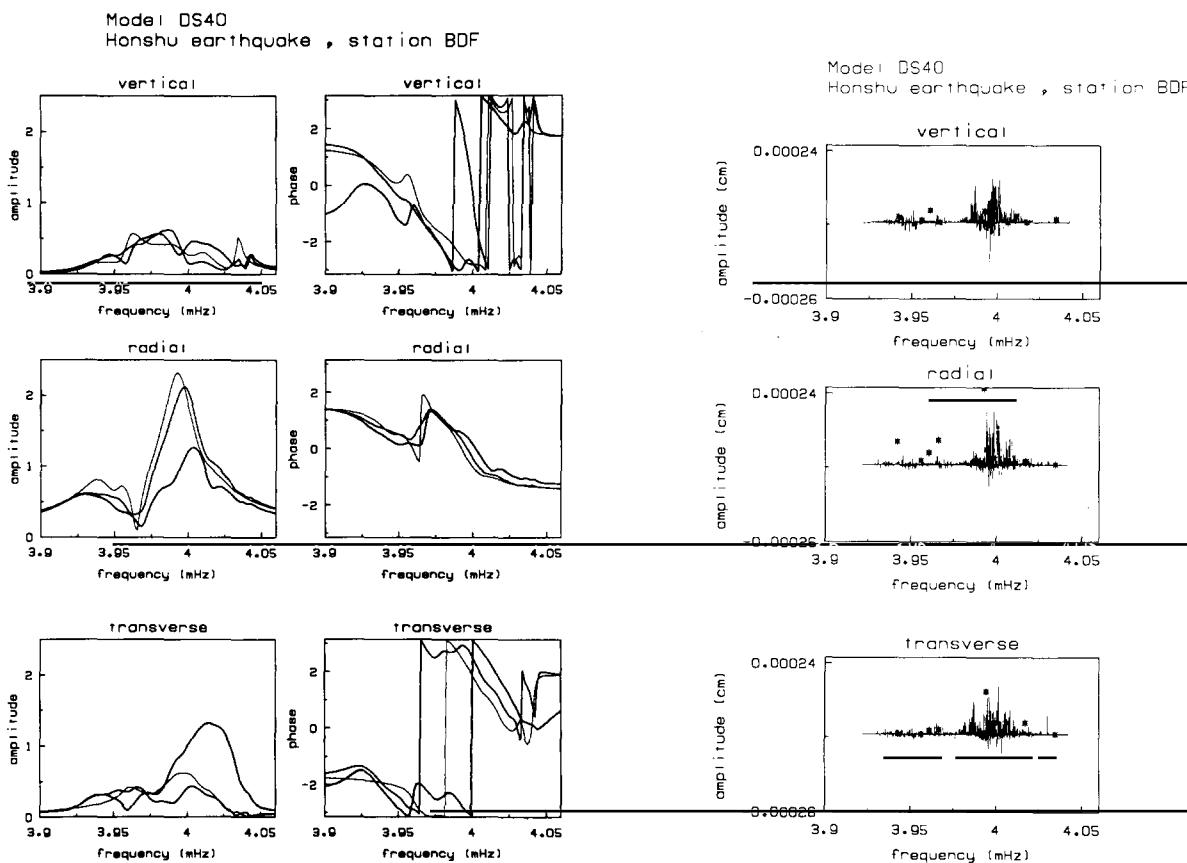


Fig. 17. (a, left) Spectra at BDF site for mechanism of Honshu deep earthquake and model DS40. Other details are the same as Fig. 14a. (b, right) Line spectra for Fig. 17a. Other details are the same as Fig. 14b.

is probably because the overtones, whose splitting is more sensitive to lateral heterogeneity than the fundamentals, have larger relative amplitudes for the deep event.

Figures 10–12 appear to show that there is substantial coupling between multiplets. On the other hand, the synthetic spectra in Figs. 14–19 do not show a gross disparity between the variational method spectra and those for a laterally homogeneous Earth. In fact, the variational spectra appear in general to show large peaks roughly where ${}_0S_{32}$ and ${}_0T_{31}$ should be. This result might appear paradoxical: if the eigenfunction of each singlet shows substantial coupling, one might expect the spectra to show comparable evidence of coupling. However, due to the smoothing effect of attenua-

tion, the coupling that can be clearly seen in the synthetic line spectra cannot be clearly seen when anelasticity is included in the synthetic spectra.

This may have potentially important implications. The fact that observed spectra seem to show distinct peaks for ${}_0S_{32}$ and ${}_0T_{31}$ is often cited as an argument against significant coupling between multiplets. However, Figs. 14–19 clearly show that anelasticity can have the effect of obscuring the underlying strong coupling that actually is occurring. Developing data processing methods to allow the recovery of data on such strong coupling is thus a major problem in observational long period seismology.

Figures 14–19 show significant differences in the phase and amplitude spectra of all three mod-

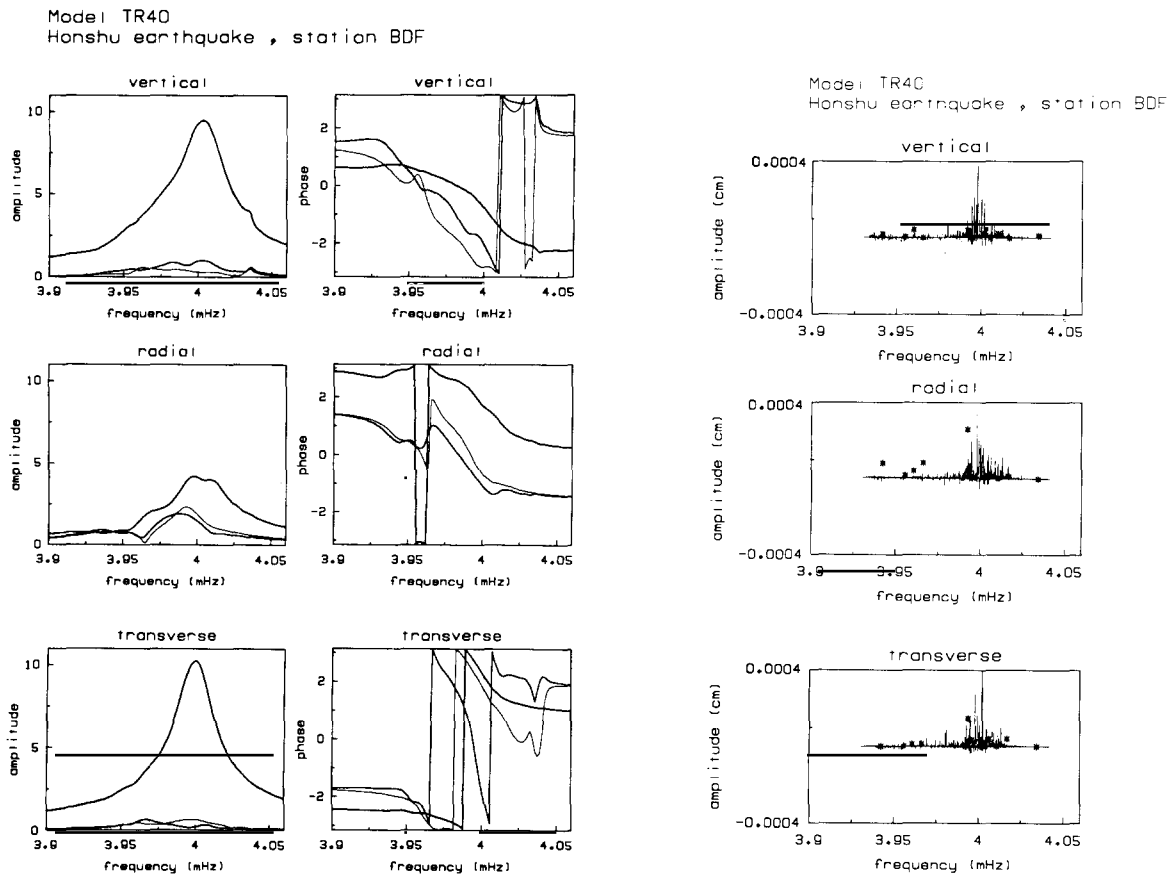


Fig. 18. (a, left) Spectra at BDF site for mechanism of Honshu deep earthquake and model TR40. Other details are the same as Fig. 14a. (b, right) Line spectra for Fig. 18a. Other details are the same as Fig. 14b.

els in nearly every plot. Also, the differences between the two models of ocean lateral heterogeneity (TR40 and OK40) are just as large as the differences between those two models and the deep heterogeneity model DS40. It should be possible, therefore, to differentiate effects of regionalization of shallow heterogeneity from effects of deep lateral heterogeneity using the information in the phase as well as the amplitude spectrum, i.e., the waveform.

10. Discussion

The synthetic spectra presented here indicate that the variational computations have the poten-

tial to distinguish between different regionalizations of lateral heterogeneity, and to resolve in the depth extent of lateral heterogeneity. Thus, the variational procedure provides a powerful tool for testing theoretical models of lateral heterogeneity in the Earth.

Acknowledgments

We used HITAC S-810/20, HITAC M-280H and VAX 11/780 computer systems at the Computer Centre of the University of Tokyo. R.J.G. was a Guggenheim Fellow during part of the period of this research. S.T. was supported by a Graduate Fellowship and by a Fellowship for

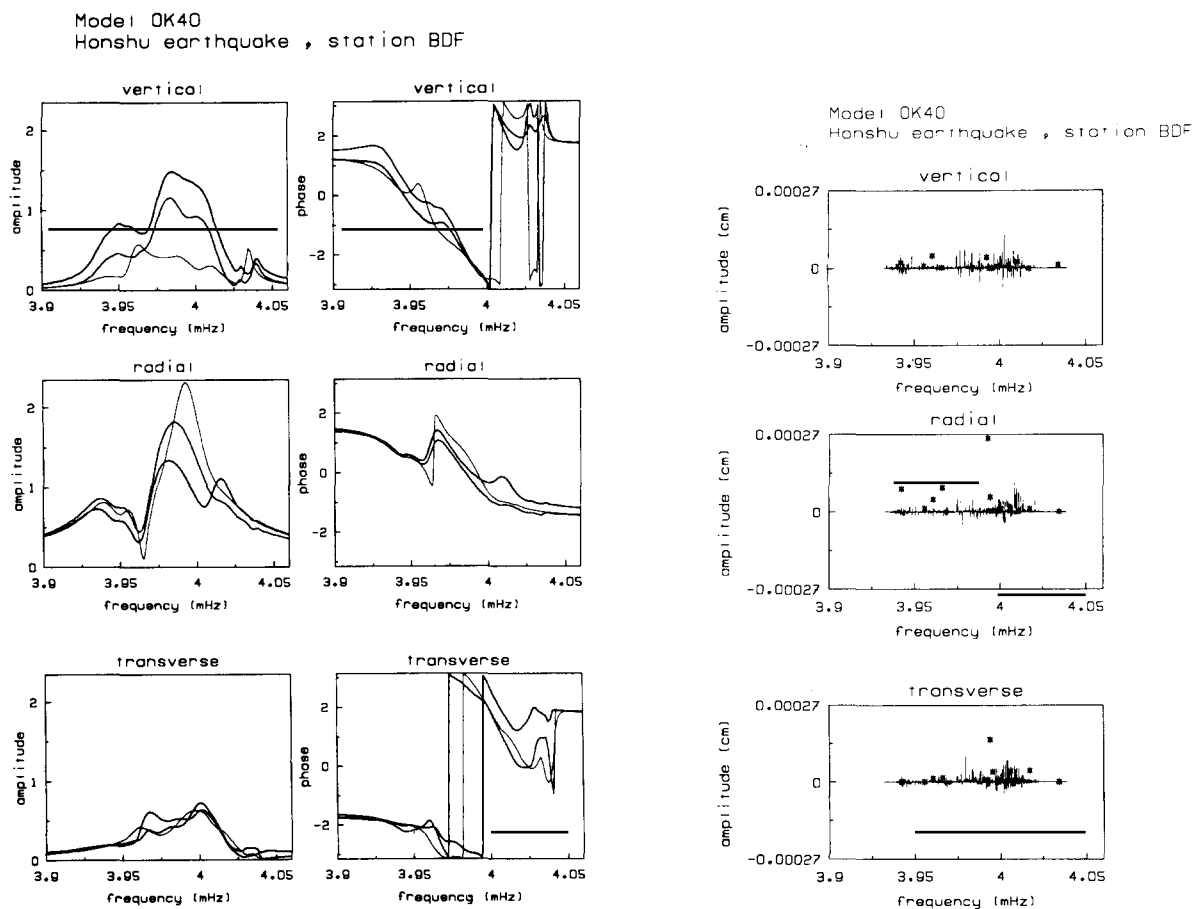


Fig. 19. (a, left) Spectra at BDF site for mechanism of Honshu deep earthquake and model OK40. Other details are the same as Fig. 14a. (b, right) Line spectra for Fig. 19a. Other details are the same as Fig. 14b.

Japanese Junior Scientists from the Japan Society for the Promotion of Science. This research was partially supported in the US by NSF Grants EAR82-18961 and EAR84-18329 and in Japan by

a Grant-in-Aid for Scientific Research from the Ministry of Education, Science and Culture (No. 60460044).

APPENDIX: MATRIX ELEMENTS

The integrals used to construct the energy matrices for the eigenvalue problem are summarized here. They are substantially the same as those of Woodhouse (1980), although they are in a slightly different form and the ellipticity integrals are somewhat different. With the exception of the angular order 2 perturbation introduced by ellipticity, it is assumed that none of the lateral variations in material properties affect the core/mantle boundary or any other liquid/solid interface. Thus, the boundary terms described by Woodhouse and Dahlen (1978) are omitted (except those related to ellipticity). If one does use a model containing lateral variations in properties at a liquid/solid interface, these terms would have to be included. In addition, the model is assumed to be locally isotropic.

Terms relating to attenuation are not given explicitly, but they can be constructed from the elasticity integrals by substituting $\kappa^{im} = \kappa Q \kappa^{-1}$ and/or $\mu^{im} = \mu Q \mu^{-1}$ for $\kappa_s^t(r)$ and $\mu_s^t(r)$, respectively (Woodhouse, 1980). Since lateral variation in the attenuation structure of the Earth is not well defined, only the effects of a spherically symmetric μ^{im} are incorporated in the work discussed in this paper. In addition, only terms for the upper halves of the energy matrices are given. The elasticity, gravitational, ellipticity, and rotational terms for the lower halves can be constructed using the Hermitian property of those terms, and the spherically symmetric attenuation terms are symmetric about the diagonals of the matrices.

Recently Geller (1987) has suggested that Woodhouse and Dahlens' (1978) energy integrals for the self-gravitation terms are incorrect. If Geller's suggestion proves to be correct, the integrals given below must be revised. However, since the results in the present paper are for modes with a period of about 250 sec, the self-gravitation terms are not important in the calculations presented in the body of this paper.

Notation and Common Terms

Let a toroidal mode of a spherically symmetric Earth model be of the form:

$$|k>_t = {}_n W_l(r) [l(l+1)]^{1/2} T_l^m(\theta, \phi) \quad |k>_t = |n, l, m>_t$$

and let spheroidal modes be of the form:

$$|k>_s = {}_n U_l(r) R_l^m(\theta, \phi) + [l(l+1)]^{1/2} {}_n V_l(r) S_l^m(\theta, \phi) \quad |k>_s = |n, l, m>_s$$

where ${}_n W_l(r)$, ${}_n U_l(r)$, and ${}_n V_l(r)$ are the solutions to the radial parts of the equations of motion, $T_l^m(\theta, \phi)$, $R_l^m(\theta, \phi)$, and $S_l^m(\theta, \phi)$ are fully normalized vector spherical harmonics:

$$T_l^m(\theta, \phi) = \frac{1}{[l(l+1)]^{1/2}} \left[0, \frac{1}{\sin\theta} \frac{\partial Y_l^m(\theta, \phi)}{\partial \phi}, -\frac{\partial Y_l^m(\theta, \phi)}{\partial \theta} \right]$$

$$R_l^m(\theta, \phi) = \left[Y_l^m(\theta, \phi), 0, 0 \right]$$

$$S_l^m(\theta, \phi) = \frac{1}{[l(l+1)]^{1/2}} \left[0, \frac{\partial Y_l^m(\theta, \phi)}{\partial \theta}, \frac{1}{\sin\theta} \frac{\partial Y_l^m(\theta, \phi)}{\partial \phi} \right]$$

and $Y_l^m(\theta, \phi)$ is an orthonormalized, complex scalar spherical harmonic as defined by Jackson (1975). The gravitational potential field associated with a spheroidal mode will be represented by ϕ_1 . In the expressions which follow, ${}_n W_l(r)$ will be abbreviated to W , ${}_n W_l(r)$ will be abbreviated to W' , and similarly for the other radial functions. Also, $\dot{W} = dW/dr$, $\dot{W}' = dW'/dr$, etc. In addition, it is assumed that the modes of the spherically symmetric model are normalized such that:

$$\langle k' | \rho_0(r) | k \rangle_t = \delta_{k'k}$$

and

$$\langle k' | \rho_0(r) | k \rangle_s = \delta_{k'k}$$

Next, expand the density, shear modulus, and bulk modulus distributions of the laterally heterogeneous model in terms of spherical harmonics:

$$\rho(r, \theta, \phi) = \sum_s \sum_{t=-s}^s \rho_s^t(r) Y_s^t(\theta, \phi) \quad , \quad \mu(r, \theta, \phi) = \sum_s \sum_{t=-s}^s \mu_s^t(r) Y_s^t(\theta, \phi)$$

$$\kappa(r, \theta, \phi) = \sum_s \sum_{t=-s}^s \kappa_s^t(r) Y_s^t(\theta, \phi)$$

In addition to these terms, the perturbations to material properties and the gravitational potential caused by ellipticity are given by Dahlen (1968) as:

$$\rho_\varepsilon(r, \theta, \phi) = \left[\frac{4\pi}{5} \right]^{1/2} \cdot \frac{2}{3} r \varepsilon(r) \frac{\partial \rho_0(r)}{\partial r} Y_2^0(\theta, \phi)$$

$$\mu_\varepsilon(r, \theta, \phi) = \left[\frac{4\pi}{5} \right]^{1/2} \cdot \frac{2}{3} r \varepsilon(r) \frac{\partial \mu_0(r)}{\partial r} Y_2^0(\theta, \phi)$$

$$\kappa_\varepsilon(r, \theta, \phi) = \left[\frac{4\pi}{5} \right]^{1/2} \cdot \frac{2}{3} r \varepsilon(r) \frac{\partial \kappa_0(r)}{\partial r} Y_2^0(\theta, \phi)$$

$$\phi_\varepsilon(r, \theta, \phi) = \left[\frac{4\pi}{5} \right]^{1/2} \left[\frac{2}{3} r \varepsilon(r) \frac{d\phi_0(r)}{dr} - \frac{1}{3} \Omega^2 r^2 \right] Y_2^0(\theta, \phi)$$

where $\varepsilon(r)$ is the ellipticity of the Earth as a function of radius, $\phi_0(r)$ is the gravitational potential energy of the Earth, and Ω is the rotational frequency of the Earth. In the following equations, $\varepsilon = \varepsilon(r)$, $\dot{\varepsilon} = d\varepsilon/dr$, and $\phi_0 = \phi_0(r)$.

Now define some constants which occur frequently:

$$a_1 = \frac{[l'(l'+1) + l(l+1) - s(s+1)]}{2}$$

$$a_2 = \frac{[l(l+1) + s(s+1) - l'(l'+1)]}{2}$$

$$a_3 = \frac{[l'(l'+1) + s(s+1) - l(l+1)]}{2}$$

$$a_4 = a_1 [l'(l'+1) + l(l+1) - s(s+1) - 2] - [l(l+1)][l'(l'+1)]$$

and, following Luh (1973, 1974) and Woodhouse (1980), define:

$$F' = \frac{2U' - l'(l'+1)V'}{r} \quad , \quad F = \frac{2U - l(l+1)V}{r}$$

$$Z' = \frac{dW'}{dr} - \frac{W'}{r} \quad , \quad Z = \frac{dW}{dr} - \frac{W}{r}$$

$$X' = \frac{(U'-V')}{r} + \dot{V}' \quad , \quad X = \frac{(U-V)}{r} + \dot{V}$$

The surface integrals to be evaluated reduce to:

$$\mathbf{I}_1 = \int_{S_1} Y_l^{m*}(\theta, \phi) Y_s^t(\theta, \phi) Y_l^m(\theta, \phi) d\Omega$$

$$= \left[\frac{(2l+1)(2s+1)}{4\pi(2l'+1)} \right]^{1/2} \langle l s 0 0 | l s l' 0 \rangle \langle l s m t | l s l' m' \rangle$$

$$\begin{aligned} \mathbf{I}_2 &= \int_{S_1} (-\hat{r} \times \nabla Y_l^{m*}(\theta, \phi)) Y_s^l(\theta, \phi) (\nabla Y_{l'}^{m'}(\theta, \phi)) d\Omega \\ &= \left[\frac{(2l+1)(2s+1)(l'+l+s+2)(l'+l+s+4)}{\pi(2l'+3)(l'+l+s+3)} (l+l'-s+1)(l+s-l'+1)(s+l'-l+1) \right]^{1/2} \\ &\quad \cdot \frac{i}{4} \cdot \langle l s m t | l s l' m' \rangle \langle (l+1)(s+1) 0 0 | (l+1)(s+1)(l'+1) 0 \rangle \end{aligned}$$

$$\begin{aligned} \mathbf{I}_3 &= \delta_{mm'} \delta_{ll'} \frac{l(l+1)-3m^2}{(2l-1)(2l+3)} + \delta_{mm'} \delta_{l(l'+2)} \frac{3}{2} \left[\frac{(l-m)(l+m)(l'+1-m)(l'+1+m)}{(2l-1)(2l+1)(2l'+3)(2l'+1)} \right]^{1/2} \\ &\quad + \delta_{mm'} \delta_{(l+2)l'} \frac{3}{2} \left[\frac{(l'-m)(l'+m)(l+1-m)(l+1+m)}{(2l'-1)(2l'+1)(2l+3)(2l+1)} \right]^{1/2} \end{aligned}$$

$$\mathbf{I}_4 = \delta_{mm'} \delta_{(l+1)l'} \left[\frac{(l'+m)(l'-m)}{(2l'+1)(2l'-1)} \right]^{1/2} + \delta_{mm'} \delta_{l(l'+1)} \left[\frac{(l+m)(l-m)}{(2l+1)(2l-1)} \right]^{1/2}$$

where $\langle l s 0 0 | l s l' 0 \rangle$, $\langle l s m t | l s l' m' \rangle$, etc., are Clebsch-Gordan coefficients (Merzbacher, 1970), * denotes the complex conjugate transpose, and S_1 is the surface of a unit sphere. \mathbf{I}_3 and \mathbf{I}_4 are essentially special cases of \mathbf{I}_1 and \mathbf{I}_2 which appear in the rotation and ellipticity integrals (for which $s = 2$).

Toroidal-Toroidal Matrix Elements

Elasticity integrals:

$$T_{k'k} = \sum_s \sum_t \int r a_1 r^2 W' W \rho_s^t(r) dr \mathbf{I}_1$$

$$V_{k'k} = \sum_s \sum_t \int r^2 \mu_s^t(r) \left[a_1 Z' Z + a_4 \frac{W' W}{r^2} \right] dr \mathbf{I}_1$$

Rotational integral:

$$C_{k'k} = \delta_{mm'} \delta_{ll'} 2 m \omega \Omega \int r \rho_0(r) W W' r^2 dr$$

Ellipticity integrals ($s = 2$ in a_1, a_2, a_3, a_4):

$$T_{k'k} = \frac{2}{3} \int r^2 a_1 (r \dot{\epsilon} + 3 \epsilon) \rho_0 W W' dr \mathbf{I}_3$$

$$\begin{aligned} V_{k'k} &= \frac{2}{3} \int r \mu_0(r) \left\{ r \epsilon \left[(a_2 l'(l'+1) + 6 a_1) \dot{W}' W + (a_3 l(l+1) + 6 a_1) W' \dot{W} \right] \right. \\ &\quad \left. - (r \dot{\epsilon} + \epsilon) \left[a_4 W' W + a_1 r^2 (Z' Z - \dot{W}' Z - \dot{W} Z') \right] - \epsilon r^2 a_1 (\dot{W}' Z + \dot{W} Z') \right\} dr \mathbf{I}_3 \end{aligned}$$

Spheroidal - Spheroidal Matrix Elements

Elasticity integrals:

$$T_{k'k} = \sum_s \sum_t \int r^2 \rho_s^t(r) (U' U + a_1 V' V) dr \mathbf{I}_1$$

$$V_{k'k} = \sum_s \sum_t \int r^2 \left\{ r^2 \kappa_s^t(r) (\dot{U}' + F') (\dot{U} + F) \right. \\ \left. + \mu_s^t(r) \left[a_4 V' V + a_1 r^2 X' X + \frac{r^2}{3} (2\dot{U}' - F') (2\dot{U} - F) \right] \right\} dr \mathbf{I}_1$$

Gravitational integrals:

$$V_{k'k} = \int r^2 \rho_0(r) \left\{ 8\pi G \rho_0(r) U' U - \frac{1}{2} \frac{d\phi_0}{dr} \left[U' F + U F' + 4 \frac{U' U}{r} \right] \right. \\ \left. + U' \dot{\phi}_1 + U \dot{\phi}_1' + \frac{a_1}{r} (V' \phi_1 + V \phi_1') + \frac{a_1}{2r} \frac{d\phi_0}{dr} (V' U + U' V) \right\} dr \mathbf{I}_1 \\ + \int r^2 \rho_0(r) \phi_s^t(r) \left\{ s(s+1) U' U + a_2 \frac{r}{2} \left[U' \dot{V} + \frac{U' V}{r} - \dot{U}' V - 2F' V \right] \right. \\ \left. + a_3 \frac{r}{2} \left[U \dot{V}' + \frac{U V'}{r} - \dot{U} V' - 2F V' \right] \right\} dr \mathbf{I}_1 \\ + \int r^2 \rho_0(r) \frac{\partial \phi_s^t}{\partial r} \left\{ a_2 \frac{U' V}{2r} + a_3 \frac{U V'}{2r} - U' F - U F' \right\} dr \mathbf{I}_1$$

Rotational integrals:

$$C_{k'k} = \delta_{ll'} \delta_{mm'} 2 \Omega \omega m \int r^2 \rho_0(r) (V' V + U V' + U' V) dr \\ V_{k'k} = \delta_{ll'} \delta_{mm'} \frac{2}{3} \Omega^2 \left[\delta_{nn'} - l(l+1) \int r^2 \rho_0(r) (V' V + U V' + U' V) dr \right]$$

Ellipticity integrals ($s = 2$ in a_1, a_2, a_3, a_4):

$$T_{k'k} = \frac{2}{3} \int r^2 \rho_0(r) \left[\varepsilon (a_3 U V' + a_2 U' V) + (r \dot{\varepsilon} + 3\varepsilon) (a_1 V V' + U U') \right] dr \mathbf{I}_3 \\ V_{k'k} = \int \frac{2}{3} r^2 \varepsilon \left[\mu_0(r) \mathbf{M} - \kappa_0(r) \mathbf{K} + \rho_0(r) \mathbf{R} \right] dr \mathbf{I}_3$$

where:

$$\mathbf{K} = (\dot{U} + F) \left[\dot{U}' + (a_3 - 2) \frac{V'}{r} \right] + (\dot{U}' + F') \left[\dot{U} + (a_2 - 2) \frac{V}{r} \right] \\ + \frac{(r \dot{\varepsilon} + \varepsilon)}{2\varepsilon} \left\{ (\dot{U} + F) \left[F' - \dot{U}' + 2 a_3 \frac{V'}{r} \right] + (\dot{U}' + F') \left[F - \dot{U} + 2 a_2 \frac{V}{r} \right] \right\}$$

$$\begin{aligned}
\mathbf{M} = & -\frac{(2\dot{U}-F)}{3} \left[2\dot{U}' + a_3 \left[3\dot{V}' - \frac{4V'}{r} \right] \right] - \frac{(2\dot{U}'-F')}{3} \left[2\dot{U} + a_2 \left[3\dot{V} - \frac{4V}{r} \right] \right] \\
& + \left[\dot{V} + \frac{(U-V)}{r} \right] \left[a_2\dot{U}' - a_1\dot{V}' - a_3 l(l+1)\frac{V'}{r} \right] + (a_3 l(l+1) + 6a_1) \frac{V'\dot{V}}{r} \\
& + \left[\dot{V}' + \frac{(U'-V')}{r} \right] \left[a_3\dot{U} - a_1\dot{V} - a_2 l'(l'+1)\frac{V}{r} \right] + (a_2 l'(l'+1) + 6a_1) \frac{V\dot{V}'}{r} \\
& - \frac{(r\dot{\epsilon} + \epsilon)}{\epsilon} \left\{ \frac{a_1}{2} \left[\left[\dot{V} + \frac{(U-V)}{r} \right] \left[\frac{(U'-V')}{r} - \dot{V}' \right] - \dot{V}' \left[\dot{V} + \frac{(U-V)}{r} \right] \right. \right. \\
& \left. \left. - \dot{V} \left[\dot{V}' + \frac{(U'-V')}{r} \right] \right] + a_4 \frac{VV'}{r^2} - \frac{(2\dot{U}-F)}{3} \left[\dot{U}' + \frac{F'}{2} - 2a_3 \frac{V'}{r} \right] \right. \\
& \left. - \frac{(2\dot{U}'-F')}{3} \left[\dot{U} + \frac{F}{2} - 2a_2 \frac{V}{r} \right] \right\} \\
\mathbf{R} = & F \left[r\dot{\phi}'_1 + 4\pi G \rho_0 rU' + \frac{d\phi_0}{dr} U' \right] + F' \left[r\dot{\phi}_1 + 4\pi G \rho_0 rU + \frac{d\phi_0}{dr} U \right] \\
& - \frac{(a_2 U'V + a_3 UV')}{r} \frac{d\phi_0}{dr} + \frac{1}{r} \left[6UU' \frac{d\phi_0}{dr} + (a_1 V - l'(l'+1)U) \phi'_1 \right. \\
& \left. + (a_1 V' - l(l+1)U') \phi_1 \right] - \frac{(r\dot{\epsilon} + 3\epsilon)}{2\epsilon} \left\{ \frac{2a_1}{r} \left[\phi_1 V' + \phi'_1 V \right] \right. \\
& \left. + U' \left[2\dot{\phi}_1 + 8\pi G \rho_0 U - a_2 \frac{2V}{r} \frac{d\phi_0}{dr} \right] + U \left[2\dot{\phi}'_1 + 8\pi G \rho_0 U' - a_3 \frac{2V'}{r} \frac{d\phi_0}{dr} \right] \right\}
\end{aligned}$$

Toroidal - Spheroidal Matrix Elements

In the expressions which follow, the toroidal mode is the "primed" mode.

Elasticity integrals:

$$T_{k'k} = \sum_s \sum_t \int r \left[r^2 \rho_s^t(r) W' V \right] \mathbf{I}_2 dr$$

$$V_{k'k} = \sum_s \sum_t \int r \left[\mu_s^t(r) \left[r^2 Z'X + 2(a_1-1) W'V \right] \right] \mathbf{I}_2 dr$$

Gravitational integrals:

$$\begin{aligned}
V_{k'k} = & \sum_s \sum_t \int r \left\{ \rho_s^t(r) \left[W'\phi_1 + \frac{1}{2} W'U \frac{d\phi_0}{dr} \right] \right. \\
& \left. - \frac{1}{2} \rho_0(r) \left[\frac{d\phi_s^t}{dr} W'U + \phi_s^t \left[UW' - W'\dot{U} - 2W'F + \frac{UW'}{r} \right] \right] \right\} dr \mathbf{I}_2
\end{aligned}$$

Rotational integral ($s = 2$):

$$C_{k'k} = 2 i \omega \Omega \delta_{m'm} \mathbf{I}_4 \int \rho_0(r) r^2 (a_3 U - a_1 V) W' dr$$

Ellipticity integral ($s = 2$):

$$T_{k'k} = 2 im \delta_{m'm} \mathbf{I}_4 \int \rho_0(r) r^2 \left[\varepsilon(W'U - 3W'V) - r \dot{\varepsilon} W'V \right] dr$$

$$V_{k'k} = 2 im \delta_{m'm} \mathbf{I}_4 \int r^2 \left\{ \rho_0(r) \mathbf{R} + \mu_0(r) \mathbf{M} - \kappa_0(r) \mathbf{K} \right\} dr$$

where:

$$\begin{aligned} \mathbf{M} &= \varepsilon \left[\dot{W}' \left[2\dot{V} - \dot{U} + \frac{3U}{r} - \frac{(2a_2+1)}{r} V \right] - \dot{V} \dot{W}' \right. \\ &\quad \left. + \frac{W'}{r} \left[7\dot{U} - 7\dot{V} + \frac{5l(l+1)}{r} V - \frac{l(l'+1)+8}{r} U \right] - \frac{W'}{r^2} (U-V) \right. \\ &\quad \left. - \frac{2W'}{3r} (2\dot{U}-F) + (2a_1-2) \frac{VW'}{r^2} \right] \\ &\quad - r \dot{\varepsilon} \left[\frac{W'}{r^2} (U-V) - (2a_1-2) \frac{W'}{r^2} V + \frac{2W'}{3r} (2\dot{U}-F) + \dot{V} \dot{W}' \right] \\ \mathbf{K} &= - (r \dot{\varepsilon} + 2\varepsilon) W' \frac{(\dot{U}+F)}{r} \\ \mathbf{R} &= \varepsilon \left[\frac{d\phi_0}{dr} \left[\frac{2}{r} W'U - \dot{W}'U - W'\dot{U} \right] + 2W' \frac{\phi_1}{r} - 4\pi G \rho_0(r) UW' \right] \\ &\quad + \dot{\varepsilon} W' \phi_1 \end{aligned}$$

Diagonals of the Energy Matrices

The terms given above all come from perturbations made to the starting spherically symmetric Earth model. Before the matrices can be used to solve for the modes of the laterally heterogeneous model, a factor of 1.0 must be added to the diagonal elements of the kinetic energy matrix and the squares of the unperturbed frequencies must be added to the appropriate diagonal elements of the potential energy matrices. This is in order to incorporate the effects of the spherically symmetric portions of the density, bulk modulus, and shear modulus. Essentially, it converts the matrices from being perturbation energy matrices to being full energy matrices for the Earth model under consideration.

Selection Rules

The number of matrix elements which must be computed is reduced considerably by applying the selection rules for the Clebsch-Gordan coefficients (Merzbacher, 1970) :

- (a) $\langle l s m t | l s l' m' \rangle = 0$ if $m + t \neq m'$
- (b) $\langle l s 0 0 | l s l' 0 \rangle = 0$ if $l + s + l'$ is odd
- (c) $l, l',$ and s must satisfy $|l - l'| \leq s \leq l + l'$

The second selection rule means that matrix elements involving unperturbed modes within the same multiplet (i.e., $n = n'$ and $l = l'$) are affected only by lateral heterogeneity of even angular order. Therefore, as Madariaga (1972) and others have noted, solutions obtained by first-order degenerate perturbation theory contain no information about lateral heterogeneity of odd angular order. Solutions obtained by the general Rayleigh-Ritz variational approach, on the other hand, do contain such information.

References

- Aki, K. and Richards, P.G., 1980. *Quantitative Seismology: Theory and Methods*. Freeman, San Francisco, vol. 1.
- Buland, R.P., 1976. Retrieving the Seismic Moment Tensor. Ph. D. Thesis, University of California, San Diego.
- Dahlen, F.A., 1968. The normal modes of a rotating elliptical Earth II. Near resonance multiplet coupling. *Geophys. J.R. Astron. Soc.*, 16: 329–367.
- Dziewonski, A. and Steim, J.M., 1982. Dispersion and attenuation of mantle waves through waveform inversion. *Geophys. J.R. Astron. Soc.*, 70: 503–527.
- Finlayson, B.A., 1972. *The method of weighted residuals and variational principles*. Academic, New York.
- Garbow B.S., Boyle, J.M., Dongarra, J.J. and Moler, C.B., 1977. *Matrix Eigensystem Routines—EISPACK Guide Extension*. Lecture Notes in Computer Science, 51, Springer-Verlag, Heidelberg.
- Geller, R.J., 1987. Elastodynamics in a laterally heterogeneous body. *J. Geophys. Res.*, submitted.
- Geller, R.J. and Stein, S., 1978. Normal modes of a laterally heterogeneous body: a one dimensional example. *Bull. Seismol. Soc. Am.*, 68: 103–116.
- Geller, R.J. and Tsuboi, S., 1987. Seismology in a heterogeneous, anelastic, rotating Earth. *J. Phys. Earth*, submitted.
- Geller, R.J., Noack, R.M. and Fetter, A.L., 1985. Normal mode solutions for absorbing boundary conditions. *Geophys. Res. Lett.*, 12: 145–148.
- Gilbert, F. and Dziewonski, A., 1975. An application of normal mode theory to the retrieval of structural parameters and source mechanisms from seismic spectra. *Philos. Trans. R. Soc. London, A* 278: 187–269.
- Jackson, J.D., 1975. *Classical Electrodynamics*. Wiley, New York, 3rd ed.
- Lancaster, P., 1966. *Lambda-Matrices and Vibrating Systems*. Pergamon Press, Oxford.
- Leeds, A.R., 1975. Lithospheric thickness in the western Pacific. *Phys. Earth Planet. Inter.*, 11: 61–64.
- Luh, P.C., 1973. Free oscillations of the laterally inhomogeneous Earth: quasi-degenerate multiplet coupling. *Geophys. J.R. Astron. Soc.*, 32: 187–202.
- Luh, P.C., 1974. Normal modes of a rotating, self-gravitating, inhomogeneous Earth. *Geophys. J.R. Astron. Soc.*, 38: 187–224.
- Madariaga, R., 1972. Toroidal free oscillations of the laterally heterogeneous Earth. *Geophys. J.R. Astron. Soc.*, 27: 81–100.
- Masters, G., Jordan, T.H., Silver, P.G. and Gilbert, F., 1982. Aspherical Earth structure from fundamental spheroidal-mode data. *Nature (London)*, 298: 609–613.
- Masters, G., Park, J. and Gilbert, F., 1983. Observations of coupled spheroidal and toroidal modes. *J. Geophys. Res.*, 88: 10285–10298.
- Merzbacher, E., 1970. *Quantum Mechanics*. Wiley, New York, 2nd ed.
- Morris, S.P., 1985. *Variational Normal Mode Computations for Laterally Heterogeneous Earth Models*. Ph. D. Thesis, Stanford University.
- Morris, S.P. and Geller, R.J., 1982. Toroidal modes of a simple laterally heterogeneous sphere. *Bull. Seismol. Soc. Am.*, 72: 1155–1166.
- Okal, E.A., 1977. The effect of intrinsic ocean upper-mantle heterogeneity on regionalization of long-period Rayleigh wave phase velocities. *Geophys. J.R. Astron. Soc.*, 49: 357–370.
- Park, J., 1985. *Applications of the Galerkin Formalism in the Coupling of the Earth's Free oscillations*. Ph. D. Thesis, University of California, San Diego.
- Silver, P.G. and Jordan, T.H., 1983. Total-moment spectra of fourteen large earthquakes. *J. Geophys. Res.*, 88: 3273–3293.
- Spudich, P. and Ascher, U., 1983. Calculation of complete theoretical seismograms in vertically varying media using collocation methods. *Geophys. J.R. Astron. Soc.*, 75: 101–124.
- Stein, S., Mills, J.M. and Geller, R.J., 1981. Q^{-1} models from data space inversion of fundamental spheroidal mode attenuation measurements. In: F. Stacey (Editor), *Anelasticity in the Earth*. *Geodynamics Series*, 4: 39–53.
- Tanimoto, T., 1982. *Coupling and Attenuation of Torsional Modes in a Heterogeneous Earth*. Ph. D. Thesis, University of California, Berkeley.
- Tsuboi, S., 1985. *Variational Calculation of the Normal Modes of a Laterally Heterogeneous Earth and its Application to Inverse Problems*. D. Sc. Thesis, Tokyo University.
- Tsuboi, S., Geller, R.J. and Morris, S.P., 1985. Partial derivatives of the eigenfrequencies of a laterally heterogeneous earth model. *Geophys. Res. Lett.*, 12: 817–820.
- Wiggins, R.A., 1976. A fast, new computational algorithm for free oscillations and surface waves. *Geophys. J.R. Astron. Soc.*, 47: 135–150.
- Woodhouse, J.H., 1980. The coupling and attenuation of nearly resonant multiplets in the Earth's free oscillation spectrum. *Geophys. J.R. Astron. Soc.*, 61: 261–283.
- Woodhouse, J.H. and Dahlen, F.A., 1978. The effect of a general aspherical perturbation on the free oscillations of the Earth. *Geophys. J.R. Astron. Soc.*, 53: 335–354.